# EMULSION-BASED PROCESSING AND CHARACTERIZATION OF BIOMIMETIC HYDROXYAPATITE MICROSPHERES BY USING CALCIUM PHOSPHATE CEMENTS

A THESIS SUBMITTED TO
THE GRADUATE SCHOOL OF NATURAL AND APPLIED SCIENCES
OF
MIDDLE EAST TECHNICAL UNIVERSITY

BY

NİLSU ÖNDİN

IN PARTIAL FULFILLMENT OF THE REQUIREMENTS
FOR
THE DEGREE OF MASTER OF SCIENCE
IN
METALLURGICAL AND MATERIALS ENGINEERING

NOVEMBER 2022

Approval of the thesis:

**EMULSION-BASED PROCESSING AND CHARACTERIZATION OF BIOMIMETIC HYDROXYAPATITE MICROSPHERES BY USING CALCIUM PHOSPHATE CEMENTS**

submitted by **NİLSU ÖNDİN** in partial fulfillment of the requirements for the degree of **Master of Science** i**n Metallurgical and Materials Engineering, Middle East Technical University** by,

Prof. Dr. Halil Kalıpçılar
Dean, Graduate School of **Natural and Applied Sciences** _____

Prof. Dr. Ali Kalkanlı
Head of the Department, **Metallurgical and Materials Eng.** _____

Prof. Dr. Caner Durucan
Supervisor, **Metallurgical and Materials Eng., METU** _____

**Examining Committee Members:**

Prof. Dr. Arcan F. Dericioğlu
Metallurgical and Materials Engineering, METU _____

Prof. Dr. Caner Durucan
Metallurgical and Materials Engineering, METU _____

Prof. Dr. Ziya Esen
Inter-Curricular Courses, Çankaya University _____

Assoc. Prof. Dr. Simge Çınar Aygün
Metallurgical and Materials Engineering, METU _____

Assist. Prof. Dr. Irmak Sargın
Metallurgical and Materials Engineering, METU _____

Date: 22.11.2022

**I hereby declare that all information in this document has been obtained and presented in accordance with academic rules and ethical conduct. I also declare that, as required by these rules and conduct, I have fully cited and referenced all material and results that are not original to this work.**

Name, Last name : Nilsu Öndin

Signature :

# ABSTRACT

## EMULSION-BASED PROCESSING AND CHARACTERIZATION OF BIOMIMETIC HYDROXYAPATITE MICROSPHERES BY USING CALCIUM PHOSPHATE CEMENTS

Öndin, Nilsu
Master of Science, Metallurgical and Materials Engineering
Supervisor: Caner Durucan

November 2022, 82 pages

Synthetic materials for bone defects have been widely used for biomedical applications. One of these materials is bioactive ceramic-based microspheres in the size range of couple 100s μm. These microspheres are used for irregular defect filling operations due to high packing efficiency. The spherical shape also increases the surface area, reactivity, and cell adhesion. The osteoconduction (bone tissue growth) is the primary concern for hard-tissue replacements and grafts. Alpha-tricalcium phosphate (α-TCP, α-$Ca_3(PO_4)_2$), a calcium orthophosphate with high solubility, is an attractive option in the powder form as a direct bone substitute material due to its cement-type reactivity setting to calcium-deficient hydroxyapatite (CDHAp, $Ca_9(HPO_4)(PO_4)_5(OH)$) in aqueous environments. The cement product is considered as a bioactive and biomimetic material due to its high chemical resemblance with the natural bone mineral. In this study, an emulsion-based microsphere formation has been accomplished by utilizing the cement nature of α-TCP, enabling shape preservation for water-based α-TCP slurry. Another structural component of the microspheres was an organic binder to improve and control the shaping ability, osteoconductivity and mechanical properties. The developed microspheres include

α-TCP:Ca-Alginate, α-TCP:Gelatin, and α-TCP:CSH (α-TCP:Calcium Sulfate Hemihydrate) that are formed using water in oil (w/o) emulsion-based system enabling size and morphology control. The microsphere formation was finalized by long-term ex-situ hydration of spheres shaped by emulsion. The effects of the emulsion parameters; stirring efficiency, temperature on the microsphere size and morphology were investigated by parametric studies. The effects of binder type, concentration, and hydration media (DI water and buffer solution) on hydration of α-TCP to CDHAp were studied by a parametrical approach. The microstructure and mechanical properties of different hybrid microspheres have been compared and reported.

Keywords: Alpha Tricalcium Phosphate, Hydroxyapatite, Gelatin, Emulsion, Microsphere

# ÖZ

## KALSİYUM FOSFAT ÇİMENTOSU KULLANILARAK BİYOMİMETİK HİDROKSİAPATİT MİKROKÜRELERİN EMÜLSİYON BAZLI İŞLENMESİ VE KARAKTERİZASYONU

Öndin, Nilsu
Yüksek Lisans, Metalurji ve Malzeme Mühendisliği
Tez Yöneticisi: Prof. Dr. Caner Durucan

Kasım 2022, 82 sayfa

Kemik kusurları için sentetik malzemeler, biyomedikal uygulamalarda yaygın olarak kullanılmaktadır. Bu malzemelerden biri de birkaç yüz μm boyut aralığındaki biyoaktif seramik bazlı mikroküreldir. Bu mikroküreler, yüksek dolgulama verimliliği nedeniyle düzensiz kusur doldurma operasyonlarında kullanılır. Küresel şekil yüzey alanını, reaktiviteyi ve hücre tutunumunu arttırır. Osteokondüksiyon (kemik dokusu büyümesi), sert doku değiştirmeleri ve greftler için temel endişe kaynağıdır. Yüksek çözünürlüğe sahip bir kalsiyum ortofosfat olan alfa-trikalsiyum fosfat (α-TCP, α-$Ca_3(PO_2)_2$), çimento tipi reaktivitesi nedeniyle doğrudan kemik nakil malzemesi olarak toz formunda uygun bir seçenektir. Sulu ortamlarda hidroksiapatit (CDHAp, $Ca_9(HPO_4)(PO_4)_5(OH)$). çimentosu, doğal kemik minerali ile yüksek kimyasal benzerliği nedeniyle biyoaktif ve biyomimetik bir malzeme olarak kabul edilmektedir. Bu çalışmada, α-TCP'nin çimento yapısından yararlanılarak, su bazlı α-TCP bulamacının şeklinin kolayca korunmasını sağlayan emülsiyon bazlı bir mikroküre oluşumu gerçekleştirilmiştir. Mikrokürelerin başka bir yapısal bileşeni, şekillendirme kabiliyetini, osteokondüksiyonu ve mekanik özellikleri daha da geliştirmek ve kontrol etmek için kullanılan organik bir

bağlayıcıdır. Geliştirilen mikroküreler, boyut ve morfoloji kontrolünü sağlayan yağ içinde su emülsiyon bazlı sistem kullanılarak oluşturulan, farklı seramik toz:bağlayıcı miktarlarına sahip α-TCP:Ca-Aljinat, α-TCP:Gelatin ve α-TCP:CSH (α-TCP:Kalsiyum Sülfat Hemihidrat) içerir. Mikroküre oluşumu, emülsiyonla şekillendirilen kürelerin uzun süreli ex-situ hidrasyonu ile sonlandırılmıştır. Emülsiyon parameteleri olan karıştırma hızı ve sıcaklığın mikroküre boyutu ve morfolojisi üzerindeki etkileri parametrik çalışmalarla incelenmiştir. Bağlayıcı türü, konsantrasyonu ve hidrasyon ortamının (DI su ve fosfat tampon çözeltisi) α-TCP'nin CDHAp'a hidrasyonu üzerindeki etkileri parametrik bir yaklaşımla incelenmiştir. Farklı hibrit mikrokürelerin mikroyapısı ve mekanik özellikleri karşılaştırmış ve rapor edilmiştir.

Anahtar Kelimeler: Alfa Trikalsiyum Fosfat, Hidroksiapatit, Jelatin, Emülsiyon, Mikroküre

To My Family

## ACKNOWLEDGMENTS

I wish to express my appreciation to my supervisor Prof. Dr. Caner Durucan for his guidance, advice, criticism, patience, encouragements, support and insight throughout the study.

I am grateful to my labmate H. Engin Sever for helping with the SEM analysis, guidance, and moral support while studying for my master's degree.

I would like to express my gratitude to all staff of the Department of Metallurgical and Materials Engineering.

I am also grateful to my childhood friend Derin Erbil for always being there for me.

Finally, I owe a depth to my mom, uncle, cousin, and grandmother for their unconditional love and unlimited support. I am deeply grateful to my family for always being my motivation with their smiling faces.

## TABLE OF CONTENTS

ABSTRACT ..... v

ÖZ ..... vii

ACKNOWLEDGMENTS ..... x

TABLE OF CONTENTS ..... xi

LIST OF TABLES ..... xiii

LIST OF FIGURES ..... xiv

CHAPTERS

1 INTRODUCTION ..... 1

2 LITERATURE REVIEW ..... 3

2.1 Natural Bone Structure and Physiology ..... 3

2.2 Bone Grafts ..... 6

2.2.1 Natural Bone Grafts ..... 6

2.2.2 Synthetic Ceramic-Based Bone Grafts ..... 7

2.3 Bone Cement ..... 14

2.3.1 Acrylic Bone Cement ..... 14

2.3.2 Calcium Sulfate Cement ..... 14

2.3.3 Calcium Phosphate (CaP) Cement ..... 16

2.3.4 Calcium Phosphate/Calcium Sulfate Cement ..... 19

2.4 Calcium Phosphate-Based Composites ..... 20

2.5 Calcium Phosphate-Based Microspheres ..... 22

2.6 Emulsion-Based Processing ..... 25

3 MATERIALS AND METHODS ..... 27
3.1 Materials ..... 27
3.2 Methods ..... 28
3.2.1 α-TCP Synthesis ..... 28
3.2.2 Production of Calcium Phosphate-Based Microspheres ..... 29
3.2.3 Material Characterization ..... 34
4 RESULTS AND DISCUSSION ..... 37
4.1 Characterization of Synthesis Products ..... 37
4.1.1 Characterization of Monetite ..... 37
4.1.2 Characterization of α-TCP ..... 40
4.2 Characterization and Properties of α-TCP/Polymer Microspheres ..... 43
4.2.1 Characterization of α-TCP/Alginate Microspheres ..... 43
4.2.2 Characterization of α-TCP/Gelatin Microspheres ..... 46
4.3 Characterization of TCP/CSH (TCP:Calcium Sulfate Hemihydrate) Hybrid Microspheres ..... 60
4.3.1 Mechanical Properties of TCP/CS Microspheres ..... 65
5 CONCLUSIONS ..... 67
REFERENCES ..... 69
APPENDICES
A. TCP/Gelatin Hydration in DI Water ..... 77
B. TCP/Gelatin Hydration in PBS ..... 80

## LIST OF TABLES

TABLES

Table 2.1: Calcium phosphates, Ca/P molar ratios of the calcium phosphates, and major properties at 25°C [24]. ..... 9
Table 3.1: Detailed preparation parameters of α-TCP/Gelatin (α-TCP/G) microspheres. ..... 32
Table 3.2: Detailed compositional information of α-TCP/CSH microspheres..... 33
Table 4.1: Viscosity of the oil phase with respect to temperature. ..... 51
Table 4.2: Natural bone properties. ..... 58
Table 4.3: Diametral tensile strength of TCP/G-5, TCP/G-7.5 and TCP/G-10. ..... 58
Table 4.4: Diametral tensile strength of hydrated TCP/G-5, CS10 and CS25..... 66

## LIST OF FIGURES

FIGURES

Figure 2.1: Schematic illustration of mineralized collagen fibril, the building block of the natural bone [6]. ..... 4
Figure 2.2: Illustration of hierarchical structural organization of natural bone from macrostructure to sub-nanostructure [6]. ..... 5
Figure 2.3: Solubility of calcium (Ca) and phosphate (P) in different calcium phosphate compounds plotted against the pH [25]. ..... 10
Figure 2.4: Phase diagram of the $CaO–P_2O_5$ (C represents CaO, and P represents ($P_2O_5$) system at elevated temperatures [29]. ..... 12
Figure 2.5: Solubility (g) of calcium sulfate hemihydrates ($CaSO_4 \cdot 12H_2O$) and calcium sulfate dihydrate $CaSO_4 \cdot 2H_2O$) at different temperatures (°C) [33]. ..... 15
Figure 2.6: Summary of apatite and brushite production by hydrolysis and acid-base interactions of different reactives [31]. ..... 18
Figure 2.7: Schematic illustration of calcium-phosphate based microsphere production routes. ..... 24
Figure 2.8: Schematic illustration of breakdown processes: creaming, flocculation, sedimentation, phase inversion, coalescence and Ostwald ripening. [56]. ..... 25
Figure 3.1: Flow chart of α-TCP synthesis procedure. ..... 29
Figure 3.2: Schematic illustration of emulsion-based processing of TCP microspheres. ..... 30
Figure 4.1: XRD diffractogram of monetite matching JCPDS card no 09-080 ..... 38
Figure 4.2: FTIR spectrum of monetite. ..... 39
Figure 4.3: SEM micrograph of monetite ($CaHPO_4$). ..... 39
Figure 4.4: XRD diffractogram of α-TCP that matches with JCPDS card no 09-348. ..... 41
Figure 4.5: FTIR spectrum of α-TCP. ..... 41
Figure 4.6: SEM micrograph of α-TCP. ..... 42

Figure 4.7: FTIR spectra of Na-Alginate solution, cross-linked α-TCP/Ca-Alginate microspheres, and pure α-TCP. ..... 44
Figure 4.8: SEM microgpraph of $\alpha$ -TCP/Alginate particles. ..... 45
Figure 4.9: FTIR spectra of α-TCP, TCP/G-5, TCP/G-7.5, TCP/G-10, and gelatin solution. ..... 47
Figure 4.10: FTIR spectra of TCP/G-5, TCP/G-7.5, TCP/G-10, and cross-linked TCP/G-5, cross-linked TCP/G-7.5, and cross-linked TCP/G-10. ..... 47
Figure 4.11: Color changes on a) TCP/G-5, b) TCP/G-7.5, and c) TCP/G-10 after cross-linking. ..... 48
Figure 4.12: SEM micrographs of a) TCP/G-10, b) TCP/G-7.5, and TCP/G-5. .... 49
Figure 4.13: SEM migrographs of a)TCP/G-5 stirred at 600 rpm, b)TCP/G-5 stirred at 1000 rpm, c)TCP/G-5 stirred at 1400 rpm, d)TCP/G-7.5 stirred at 600 rpm, e) TCP/G-7.5 stirred at 1000 rpm, f) TCP/G-7.5 stirred at 1400 rpm, g)TCP/G-10 stirred at 600 rpm, h)TCP/G-7.5 stirred at 1000 rpm, and i)TCP/G-10 stirred at 1400 rpm. ..... 50
Figure 4.14: SEM micrographs of a)TCP/G-5 at 25 °C, b) TCP/G-5 at 37 °C, c) TCP/G-7.5 at 25 °C, d) TCP/G-7.5 at 37 °C, e) TCP/G-10 at 25 °C, and f)TCP/G-10 at 37 °C. ..... 52
Figure 4.15: The XRD diffractograms of 12 h and 24 h hydrated TCP/G-5, TCP/G-7.5, and TCP/G-10. ..... 54
Figure 4.16. SEM micrograph of 24 h hydrated TCP/G-5 microsphere. ..... 54
Figure 4.17: XRD diffractograms of 6 h hydrated TCP/G-5, TCP/G-7.5, TCP/G-10 in phosphate buffer solution. ..... 56
Figure 4.18: FTIR spectra of hydrated TCP/G-5, TCP/G-7.5, and TCP/G-10. ..... 56
Figure 4.19: Diametral tensile strength data of non-hydrated TCP/G-5, TCP/G-7.5, and TCP/G-10. ..... 59
Figure 4.20: Diametral tensile strength data of hydrated TCP/G-5, TCP/G-7.5, and TCP/G-10. ..... 59

Figure 4.21: XRD diffractograms of CS25 powder, as-prepared CS25 microspheres as-prepared, hydrated CS25 microspheres for 48h in $H_2O$, and hydrated CS25 microspheres for 48 h in PBS. ..... 62
Figure 4.22: XRD diffractograms of CS25 powder, as-prepared CS25 microspheres as-prepared, hydrated CS25 microspheres for 48 h in $H_2O$, and hydrated CS25 microspheres for 48 h in PBS. ..... 62
Figure 4.23: SEM micrograph of hydrated CS10. ..... 63
Figure 4.24: SEM micrograph of hydrated CS25. ..... 63
Figure 4.25: FTIR spectra of CS25, and its hydration products in different aqueous media ($H_2O$ and PBS). ..... 64
Figure 4.26: Diametral tensile strength of hydrated TCP/G-5, CS10, and CS25. ..... 66
Figure A.1: The XRD diffractograms as a function of reaction time for TCP/G-5 in DI water. ..... 77
Figure A.2: The XRD diffractograms as a function of reaction time for TCP/G-7.5 in DI water. ..... 78
Figure A.3: The XRD diffractograms as a function of reaction time for TCP/G-10 in DI water. ..... 79
Figure B.1: The XRD diffractograms as a function of reaction time for TCP/G-5 in PBS. ..... 80
Figure B.2: The XRD diffractograms as a function of reaction time for TCP/G-7.5 in PBS. ..... 81
Figure B.3: The XRD diffractograms as a function of reaction time for TCP/G-10 in PBS. ..... 82

# CHAPTER 1

# INTRODUCTION

Biocompatible materials such as metals, ceramics, polymers, and their composites have been widely used in biomedical applications. Bone defects caused by aging, bone diseases (osteosarcoma, osteoporosis), and accidents require bone implants or fillers. The most substantial factor in the selection of materials is their compatibility with new bone formation. In this regard, natural and synthetic biomaterials with biologically, structurally, and mechanically compatible properties have been worth investigation.

Natural bone's building blocks are mineralized collagen fibers, and the mineralized part is referred to as dahllite. Dahllite is hydroxyapatite (HAp, $(Ca_{10}(PO_4)_6(OH)_2)$ with substitutions. Thus, calcium phosphate-based synthetic and biocompatible materials with the similar chemical structure to natural bone has a good level of functionality in clinical applications. Calcium phosphate-based materials are reinforced with natural and synthetic polymers to enhance the mechanical properties of the implants and fillers.

Natural polymers such as gelatin are favorable options as biopolymers due to their similar characteristics with the natural bone's organic collagen matrix and completely resorbable feature. Biomaterial's shape is another concern apart from its mechanical properties. Microspheres' flowability makes them a proper filler for irregularly shaped defects with their high surface area that enable mineral deposition and cell attachment compared to blocks and granules. Size, shape, and porosity are manipulated by shaping processes. Thus, the shaping procedure is an important parameter as it affects the morphology.

**Objective and Rationale of the Thesis**

Bone defects caused by diseases or trauma require biomedical applications to heal the bone tissue. Natural and synthetic bone substitutes have been used to fill the irregularly shaped defects. Biocompatibility and mechanical properties are the main considerations of synthetic bone materials. The resorption rate of the material *in vivo* is directly influenced by its chemical composition. Natural bone is composed of mineralized collagen tissue. The mineral part is hydroxyapatite (HAp, $Ca_{10}(PO_4)_6(OH)_2$) Therefore, calcium phosphate-based composites with natural polymers are the most appropriate options that mimic the natural bone chemistry.

Alpha-TCP, a highly soluble material that sets into apatitic CDHAp and hardens in aqueous environments, is a suitable option to replace the mineral part. Natural polymers, especially collagen derivative gelatin, are favorable options to imitate the collagen tissue with their non-toxic bioresorbable characteristics. Since the new bone formation rate depends on the interaction with the biomaterial, the surface area of the material has an important role. The surface area and morphology of the material are modified by shaping processes. Pre-shaped microspheres provide suitable space within and between themselves. The flowability of the microspheres improve the injectability, as well. $\alpha$-TCP/Alginate, $\alpha$-TCP/Gelatin, and $\alpha$-TCP/CSH/Gelatin composite microspheres with different compositions were produced by emulsion-based processing to produce a biocompatible and mechanically suitable material. Temperature, viscosity, and mixing speed effects on the morphology were studied on $\alpha$-TCP/Gelatin microspheres by changing the parameters in the emulsion.Pre-synthesized $\alpha$-TCP powders were combined with alginate, gelatin, and calcium sulfate hemihydrate ($CaSO_4 \cdot {}^1/_2H_2O$)/gelatin in order to produce composite microspheres. Effects of alginate, gelatin, and CSH compositions on morphology and hydration were investigated. Hydration products of each composition in both water and ionic aqueous solution PBS (phosphate buffer solution) were comparatively analyzed every few hours.

# CHAPTER 2

# LITERATURE REVIEW

## 2.1 Natural Bone Structure and Physiology

Bone, a hierarchical composite material, is the main compartment of the skeletal system amongst cartilage, ligament, and other connective tissues [1]. Bone's primary functions are mechanical support, load carrying, providing movement, protection of internal organs, mineral homeostasis, and blood cell production [2, 3]. Bone's elementary unit is composite mineralized collagen fibrils [4]. The bone composite consists of two main phases: inorganic (mineral) and organic (protein) [1]. The elementary unit of natural bone is shown in Figure 2.1. Inorganic phase is 60-70 wt.% of natural bone, and is mainly composed of calcium-deficient apatite that is referred to as hydroxyapatite ($(Ca_{10}(PO_4)_6(OH)_2$) with incorporating impurities such as carbonate ($CO_3^{2-}$), citrate ($C_6H_5O_7^{3-}$), sodium (Na), magnesium (Mg) and other traces (Cl, $F^-$, $K^+$, $Sr^{2+}$, $Pb^{2+}$, $Zn^{2+}$, $Cu^{2+}$, $Fe^{2+}$) [1, 3, 5]. Natural bone mineral containing carbonate is called carbonated-hydroxyapatite or dahllite [4]. Different mineralization degrees show different mechanical properties [6]. Increasing mineral content increases the stiffness and mechanical properties of the bone [5]. Organic phase is mainly Type-I collagen fibrils (20-25 wt.%) with the presence of non-collagenous proteins, polysaccharides, lipids, and primary bone cells in small quantities (3-5 wt.%) [7]. The Type-I collagen molecules are aligned as triple helices and generate interfibrillar and intrafibrillar spaces for minerals to deposit [8]. The partial elasticity and higher tensile strength of the bones are the due to these biopolymers [7]. Apart from mineral and protein constituents of bone, water is present within the collagen fibers and pores [5]. Abundant water is responsible for viscoelastic properties, nutrient diffusion, and cell activities [3, 9].

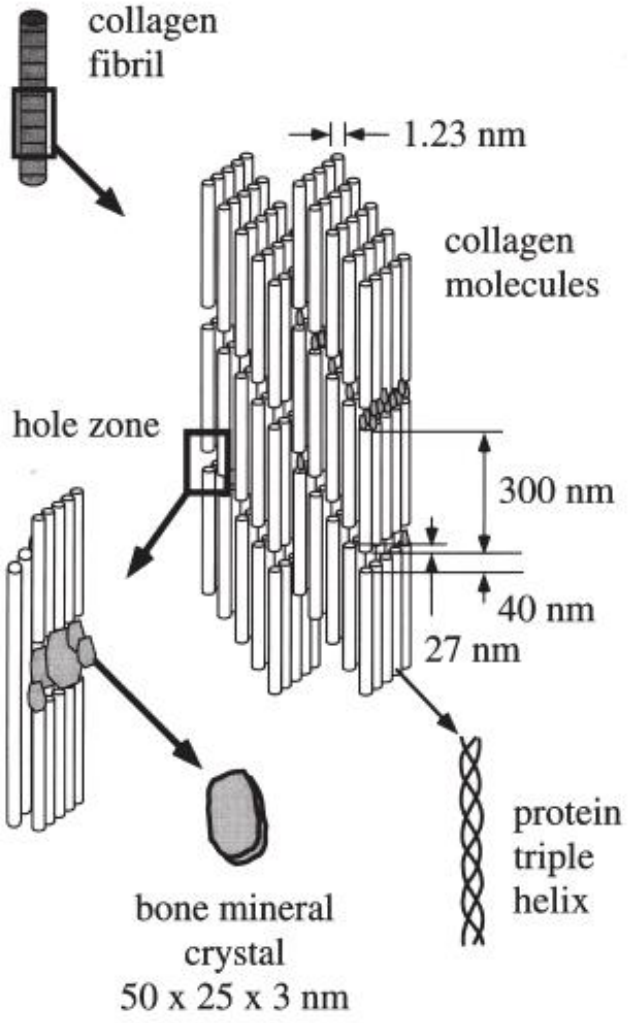



Figure 2.1: Schematic illustration of mineralized collagen fibril, the building block of the natural bone [6].

Bone is structurally divided into two subcategories: spongy (trabecular, cancellous), and cortical (compact, dense). The trabecular bone is an extensive network of plates and rods that are interconnected. Mineralized collagen fibers form lamellae and osteons (Haversian system) which are building blocks of the compact bone [6].

Human skeleton is made of 20% trabecular bone and 80% cortical bone [2]. Cortical bone is dense, less porous (6%), and contains fewer blood vessels [10]. Its tensile and compressive strength are relatively higher than trabecular bone. Trabecular bone is a foam-like porous (80%) structure and contains more blood vessels than compact bone with a higher internal surface [3, 10]. The hierarchical structure of bone is illustrated in Figure 2.2.

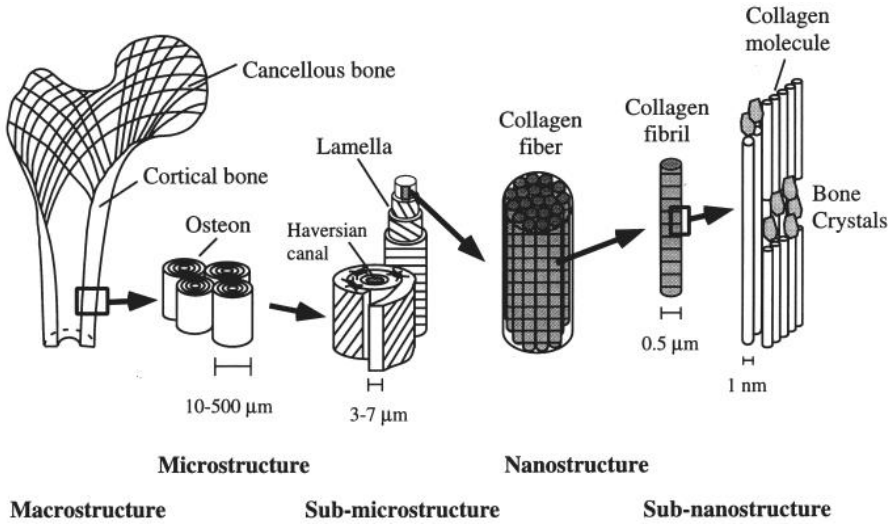



Figure 2.2: Illustration of hierarchical structural organization of natural bone from macrostructure to sub-nanostructure [6].

Bones are categorized into four shapes: irregular, long, short, and flat. Each shape includes different ratios of trabecular and compact parts [2]. The organization of the organic matrix, amount of component and arrangement of trabecular and compact bones results in various micro and macro-structural properties in the skeletal system satisfying the needs in each compartment. Therefore, each part of the skeletal system shows different characteristics.

Bone's other characteristic feature is its continual remodeling process. Remodeling is bone resorption followed by bone formation. Remodeling maintains its mineral homeostasis and repairs micro-damages [11]. Bone resorbing cells, osteoclasts, are responsible for mineral dissolution, releasing the stored calcium and digestion of the organic matrix. Bone-forming cells, osteoblasts, continue the remodeling process after the resorption by synthesizing a new bone matrix. Thus; skeletal function, homeostasis, and structure are preserved [2].

## 2.2 Bone Grafts

Natural and synthetic bone-graft substitutes have been widely used for bone defect treatments caused by trauma, infections or, bone diseases for decades. Immunological rejection is the primary concern after treatment with bone grafts. Osteogenesis, bone formation, is the major issue to prevent immunogenicity and rejections.

### 2.2.1 Natural Bone Grafts

An autograft is a bone graft that is harvested from the same individual. Autologous bone grafts provide osteogenic, osteoinductive, and osteoconductive properties as well as reliable mechanical support. Immunological rejection and infection risks are avoided in autografts [14]. Nevertheless, the limitations of autologous bone grafts are limited availability and donor-site morbidity [13, 15]. Allograft (allogenic bone graft) is an alternative bone graft to autograft harvested from either living or nonliving human donors. Unlimited availability and lack of additional surgical sites are advantages of allografts compared to autografts [14]. Infection and disease transmission risks are primary concerns with allografts. However, sterilization and storage techniques decrease its osteoinductive properties. The freeze-drying method removes water from the tissue, destroys cells, and decreases mechanical resistance [13, 14]. Xenograft, bone grafts that originated from other species than humans, is

another type of natural bone graft due to their mechanical properties, low cost, and availability. Porcine bone, bovine bone and coral are mainly used as xenografts. Porcine and bovine-based xenografts are argumentative due to possible disease transmission from animals to humans. Coral-based products composition is dissimilar to human bone and needs transformation to hydroxyapatite or other processes to enhance growth [14]. In addition to clinical complications, ethical and religious concerns are limitations in the use of xenografts [16].

### 2.2.2 Synthetic Ceramic-Based Bone Grafts

Synthetic bone grafts are developed for bone-tissue engineering due to natural bone grafts' donor-site morbidity, disease transmission, and limited availability concerns. Metals, polymers, ceramics, and their composites have been used clinically for several decades. Among them, synthetic ceramic-based bone grafts are superior alternatives to natural bone grafts due to their osteoconductivity [17]. Ceramic-based materials are in several forms: powders, pellets, and coatings[18]. Calcium sulfate (CS) and calcium phosphate (CP) and their compounds are ceramic-based, biocompatible, and osteoconductive synthetic bone graft materials [19].

#### 2.2.2.1 Calcium Sulfates

Calcium sulfate (CS) is a widely available synthetic bone graft material that has been used for decades. CS is a biocompatible, biodegradable and, osteoconductive material with a rapid setting feature and low curing temperature [20]. CS is available in powder, pellet and, cement forms. Cement form is mostly preferred for bone defect filling applications. Calcium sulfate hemihydrate (CSH) powder and its cement derivative calcium sulfate dihydrate (CSD) both demonstrate excellent biocompatibility. However, CS's resorption rate is faster than new bone formation. The rapid resorption rate of CS results in undesired gaps that cause a significant decrease in mechanical properties [21].

#### 2.2.2.2 Calcium Phosphates

Calcium phosphates (CaP) are promising candidates as synthetic bone substitute materials due to their chemical and structural similarity to natural bone and teeth. Calcium phosphates have been used for dental applications since the1970s and orthopedics since the 1980s [22].

CaPs are biocompatible, non-toxic, and biologically active materials when integrated into living tissue. Osteoconductive properties of CaP support osteoblast activities for new bone formation [23].Calcium phosphates are in different mineral compositions and exhibit different characteristics according to their Ca/P molar ratio. Different properties of several calcium phosphate compounds are shown in Table 2.1 based on their Ca/P ratios.

Solubility and stability of CaPs depend on the pH and temperature of the aqueous solution. Since the resorption rate of synthetic bone substitute materials is the main issue, most suitable CaP should be chosen for the biomedical application. Solubility diagram of CaP compounds at diffent pH values are shown in Figure 2.3.

Among the listed CaPs in Table 1, compounds with Ca/P ratio lower than 1 exhibit higher solubility but acidity. Compounds with higher Ca/P ratio than 1.67 show high basicity. Therefore, compounds with Ca/P ratio in the range of 1-1.67 among other compounds are suitable options. Considering the physiological conditions of the body; hydroxyapatite (HAp), and tricalcium phosphate (TCP)-based compounds are the most suitable ones for biomedical applications.

Table 2.1: Calcium phosphates, Ca/P molar ratios of the calcium phosphates, and major properties at 25°C [24].

| Ca/P | Formula | Solubility, $-\log(K_s)$ | Solubility, g/L | pH stability |
|---|---|---|---|---|
| 0.5 | $Ca(H_2PO_4)_2 \cdot H_2O$ | 1.14 | ~18 | 0.0–2.0 |
| 0.5 | $Ca(H_2PO_4)_2$ | 1.14 | ~17 | >100 °C. |
| 1.0 | $CaHPO_4 \cdot 2H_2O$ | 6.59 | ~0.088 | 2.0–6.0 |
| 1.0 | $CaHPO_4$ | 6.90 | ~0.048 | >100 °C. |
| 1.33 | $Ca_8(HPO_4)_2(PO_4)_4 \cdot 5H_2O$ | 96.6 | ~0.0081 | 5.5–7.0 |
| 1.5 | α-$Ca_3(PO_4)_2$ | 25.5 | ~0.0025 | Cannot ppt. |
| 1.5 | β-$Ca_3(PO_4)_2$ | 28.9 | ~0.0005 | Cannot ppt. |
| 1.0–2.2 | $Ca_xH_y(PO_4)_z \cdot nH_2O$, n = 3–4.5; 15–20% $H_2O$ | -. | -. | ~5–12 |
| 1.5–1.67 | $Ca_{10-x}(HPO_4)_x(PO_4)_{(6-x)}(OH)_{(2-x)}$ $(0 < x < 1)$ | ~85.1 | ~0.0094 | 6.5–9.5 |
| 1.67 | $Ca_{10}(PO_4)_6(OH)_2$ | 116.8 | ~0.0003 | 9.5–12 |
| 1.67 | $Ca_{10}(PO_4)_6F_2$ | 120.0 | ~0.0002 | 7–12 |
| 1.67 | $Ca_{10}(PO_4)_6O$ | ~69 | ~0.087 | Cannot ppt |
| 2.0 | $Ca_4(PO_4)_2O$ | 38–44 | ~0.0007 | Cannot ppt. |

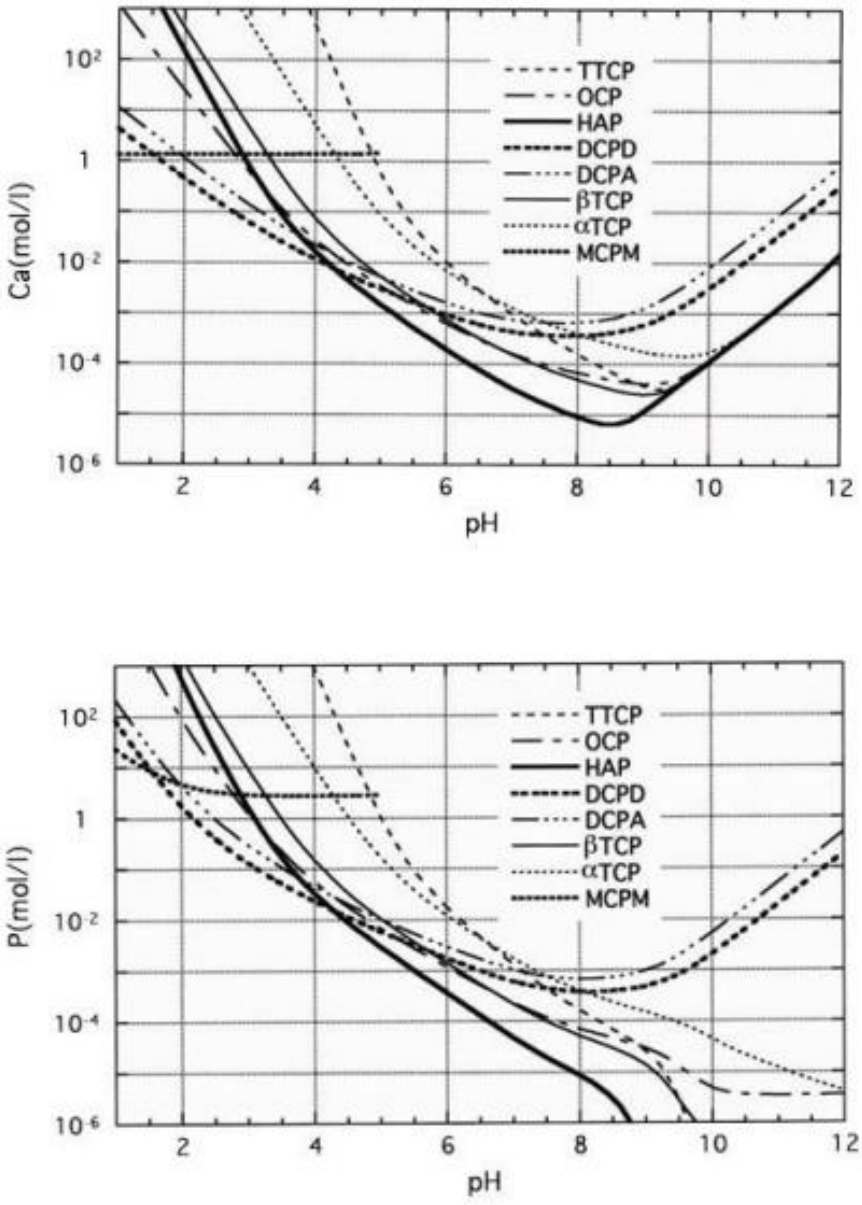



Figure 2.3: Solubility of calcium (Ca) and phosphate (P) in different calcium phosphate compounds plotted against the pH [25].

#### 2.2.2.2.1 Hydroxyapatite

Hydroxyapatite ($Ca_{10}(PO_4)_6(OH)_2$ is the primary component of bone. HAp's chemical similarity to the natural bone and teeth makes it a widely used material for biomedical applications as coatings and fillers. Synthetic HAp exhibits non-toxic, osteoconductive, and excellent biocompatible features. Among the calcium phosphates, HAp is the most stable and least soluble calcium phosphate under physiological conditions.

Stoichiometric pure hydroxyapatite has a 1/67 molar ratio and its crystal structure is monoclinic *($P2_1/b$)* at ambient conditions. However, monoclinic to hexagonal ($P6_3/m$) phase transformation occurs above 250 °C. Impurities stabilize the hexagonal structure of HAp, as well [26].

Techniques used in HAp preparation: dry, wet, and high-temperature. Products show different physical, chemical, and mechanical properties depending on the method it is synthesized. The morphology, crystallinity degree, phase purity, stoichiometry, size, and size distribution of HAp is effected by the synthesis procedure.

#### 2.2.2.2.2 Calcium-Deficient Hydroxyapatite

Calcium-deficient hydroxyapatite (CDHAp) has a non-stoichiometric formula $Ca_{(10-x)}(HPO_4)_x(PO_4)_{(6-x)}(OH)_{(2-x)}$, where $0>x>1$. Calcium deficient structure is more disordered and less stable compared to HAp. Due to a lack of stability, CDHAp has high solubility and resorption rates. The non-stoichiometric structure is suitable for ion substitutions ($Na^+$, $K^+$, $CO_3^2$, $Cl^-$ etc.) from chemicals used for preparation. Thus, CDHAp's chemical similarity to real bone increases [27].

#### 2.2.2.2.3 Tricalcium Phosphates

Tricalcium phosphate (TCP) is a bioresorbable and biocompatible material with a Ca/P molar ratio of 1.5. The chemical composition of TCP is $Ca_3(PO_4)_2$. Three polymorphs of TCP are; α'- $Ca_3(PO_4)_2$ (α'-TCP), α- $Ca_3(PO_4)_2$ (*α*-TCP) and β- $Ca_3(PO_4)_2$ (*β*-TCP). α'- TCP completely converts to α- $Ca_3(PO_4)_2$ under 1430 °C. The stable phase at room temperature is β-TCP and it is convertible to α-TCP at 1125 °C. Both β-TCP and α-TCP are used in biomedical applications [28]. Even though they all have the same composition, their crystal structure and solubility are different.

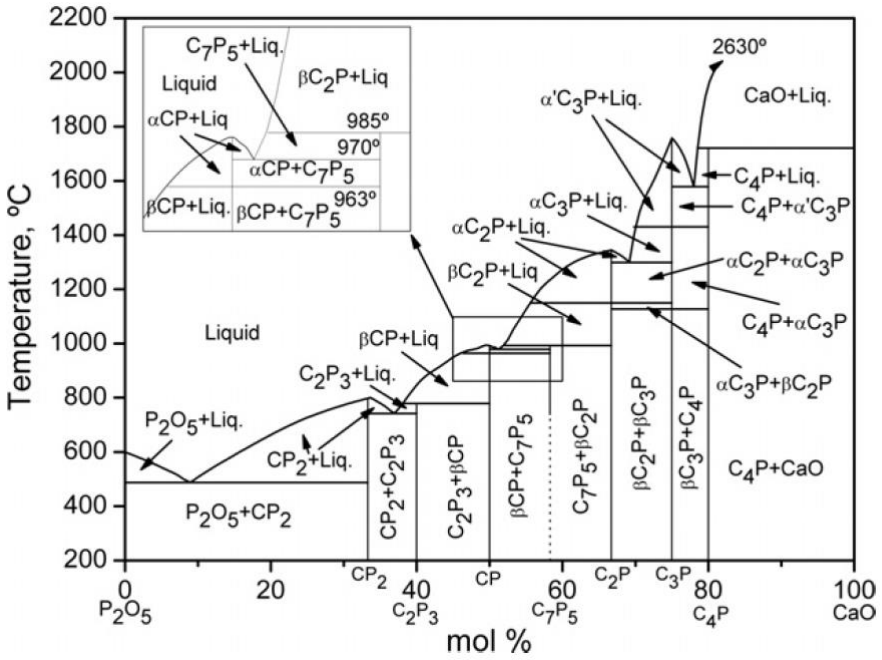



Figure 2.4: Phase diagram of the CaO–$P_2O_5$ (C represents CaO, and P represents ($P_2O_5$) system at elevated temperatures [29].

#### 2.2.2.2.3.1 β-Tricalcium Phosphate

β-tricalcium phosphate (β-TCP) is a bone substitute material with osteoconductive, biocompatible, and bioresorbable properties. β-TCP is mainly used as dense macro-porous granules and blocks [29]. Its porous structure induces the ingrowth of tissues. β-TCP's resorption by osteoclasts is slower than calcium sulfates and faster than HAp. β-TCP offers better mechanical properties when used together with HAp in biphasic form [27].

#### 2.2.2.2.3.2 α-Tricalcium Phosphate

α-Tricalcium phosphate (α-TCP) is a high-temperature stable phase of TCP and it is metastable at room temperature. Pure α-TCP is less stable and more soluble than β-TCP [27]. α-TCP's is used mainly in fine powder form and its reactivity in aqueous environments makes it a suitable solid phase for cement. When α-TCP is introduced to water, it undergoes a cement-type reaction and converts to CDHAp [30]. Conversion to CDHAp is more favorable than conversion to HAp due to CDHAp's chemical resemblance to natural bone. The setting reaction is given below in Equation 1.

$$3\ \alpha - Ca_3(PO_4)_2 + H_2O \rightarrow Ca_9HPO_4(PO_4)_5(OH) \quad (1)$$

Pure α--TCP is synthesized through different methods. Thermal transformation of a precursor, solid-state reaction, and self-propagating high-temperature synthesis are the methods used to obtain α-TCP. The solid-state reaction of solid precursors is carried out by heating precursors that are previously milled together to increase their contact area. Thermal transformation is the heating process of a CaP with a Ca/P molar ratio of 1.5. Thermal transformation of β-TCP to α-TCP at temperatures above 1125 °C is the most direct route among others [29].

## 2.3 Bone Cement

Bone cement (BC) are injectable or moldable systems with self-setting characteristics at physiological conditions for irregular-shaped bone defects. Self-setting bone cement are obtained by mixing a biocompatible powder material with a liquid. The powder/liquid mixture sets into a viscous paste then transforms into a hardened solid mass. Bone cement are divided into three groups: acrylic bone cement (ABC), calcium sulfate cement (CSC), and calcium phosphate cement (CPC) according to their chemical composition [31].

### 2.3.1 Acrylic Bone Cement

Acrylic bone cement (ABC), a biocompatible material with superior mechanical properties, is suitable for load-bearing applications. ABC is obtained by the polymerization reaction of poly-methylmethacrylate (PMMA). PMMA powder with a radiospacifying agent (barium sulfate, zirconium oxide or benzoyl peroxide) mixed with liquid methyl methacrylate (MMA) containing catalyst N, N—Dimethyl-p-toluidine (DmpT) phase [31]. During the stated exothermic polymerization reaction, the temperature may exceed 100 °C. Elevated temperature lead to thermal necrosis of the living tissue [32]. Apart from cell denaturation concern, PMMA's bioinert characteristic makes it unsuitable for non-load-bearing applications.

### 2.3.2 Calcium Sulfate Cement

Calcium sulfate cement (CSC) is developed by mixing calcium sulfate hemihydrate (CSH, $CaSO_4 \cdot {}^1/_2H_2O$) powder with a diluent [32]. Obtained paste is calcium sulfate dihydrate (CSD, $CaSO_4 \cdot 2H_2O$). Described cement- type reaction is;

$$CaSO_4 \cdot {}^1/_2H_2O + {}^3/_2H_2O \rightarrow CaSO_4 \cdot 2H_2O \quad (2)$$

CSH sets and hardens into CSD due to CSD's thermodynamically more stable characteristic in aqueous environments. CSH sets and hardens based on the dissolution-precipitation mechanism. CSH's exposure to water results in the dissolution of CSH to reach equilibrium and supply $Ca^{2+}$ and $SO_4^{2-}$ ions.

Aqueous media is supersaturated with CSD due to its lower solubility, and ions precipitate as CSD. Formed CSD set and harden in needle-like crystals. Resultant CSD's high solubility in body fluid causes rapid resorption. Dissolved CSD elevates the concentration of $Ca^{2+}$ in the body fluid. Elevated $Ca^{2+}$ concentrations tend to precipitate as a hydroxyapatite-like crystal [33]. However, absorption of CSC before new bone formation can lead to tissue degradation at and around the implantation site.

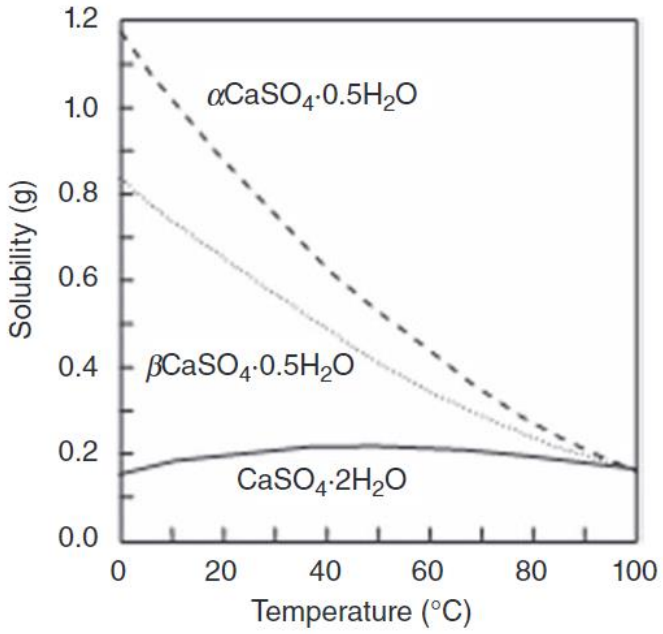



Figure 2.5: Solubility (g) of calcium sulfate hemihydrates ($CaSO_4 \cdot {}^1/_2H_2O$) and calcium sulfate dihydrate $CaSO_4 \cdot 2H_2O$) at different temperatures (°C) [33].

### 2.3.3 Calcium Phosphate (CaP) Cement

Calcium phosphate cement (CPC) is the most suitable bone cement among others because of its chemical resemblance to natural bone and mechanical properties [34]. CPC is formed by one or more calcium phosphate powders with an aqueous phase forming a paste that sets and hardens into a solid mass. The cement-type reaction of CPCs is based on the dissolution-precipitation mechanism. Even though the powder phase formulations of CPCs vary, only two final products are possible: brushite (dicalcium phosphate dihydrate, DCPD) and hydroxyapatite (HAp) and/or calcium-deficient hydroxyapatite (CDHAp) [35]. Acid-base reactions and hydrolysis are the main chemical routes to obtain brushite and CDHAp end products.

#### 2.3.3.1 Brushite-Based CaP Cement

Brushite (dicalcium phosphate dihydrate, DCPD, $4CaHPO_4{\cdot}2H_2O$) is the slightly acidic end product of acid-base interaction of almost neutral, slightly basic β-TCP with acidic monocalcium phosphate monohydrate (MCPM, $Ca(H_2PO_4)_2{\cdot}H_2O$) in water [36]. Brushite cement sets via the reaction:

$$\beta - Ca_3(PO_4)_2 + Ca(H_2PO_4)_2 \cdot H_2O + 7H_2O \rightarrow 4CaHPO_4 \cdot 2H_2O \quad (3)$$

Reaction product brushite is stable at pH<4.2 [31]. Therefore, its solubility at physiological conditions is greater than apatite. However; due to brushite's metastable property in physiological conditions, brushite to apatite transformation may happen *in vivo* [34].

#### 2.3.3.2 Apatite-Based CaP Cement

Apatite (CDHAp) is the least reactive, more stable product of calcium phosphate cement reactions. Acid-base reaction and hydrolysis are both followed as chemical routes to obtain apatite.

Brown and Chow cement is the basic acid-base interaction to obtain apatite. Slightly acidic anhydrous dicalcium phosphate (DCP, $CaHPO_4$) and basic tetracalcium phosphate (TTCP, $Ca_4(PO_4)_2O$) react to precipitate slightly basic HAp in an aqueous environment [37]. Initially formed hydroxyapatite shown in Equation 4, may further interact with the remaining DCP to form calcium-deficient hydroxyapatite (CDHAp) [36].

$$2Ca_4(PO_4)_2O + 2CaHPO_4 \rightarrow Ca_{10}(PO_4)_6(OH)_2 \quad (4)$$

The hydration process is the dissolution-precipitation of a calcium phosphate compound to convert to another with the same Ca/P molar ratio in an aqueous environment (.Cement powders α-TCP, β-TCP, and TTCP, all tend to precipitate as CDHAp upon contact with water [36]. α-TCP hydration is shown in Equation 5.

$$\alpha - Ca_3(PO_4)_2 + H_2O \rightarrow Ca_9(HPO_4)(PO_4)_5(OH) \quad (5)$$

Hydration product CDHAp is a stable product *in vitro* pH-adjusted conditions (stable at pH>4.2) [31]. Under physiological conditions, due to the presence of carbonate ions ($CO_3^{2-}$) in body fluids, carbonated apatite forms [36].

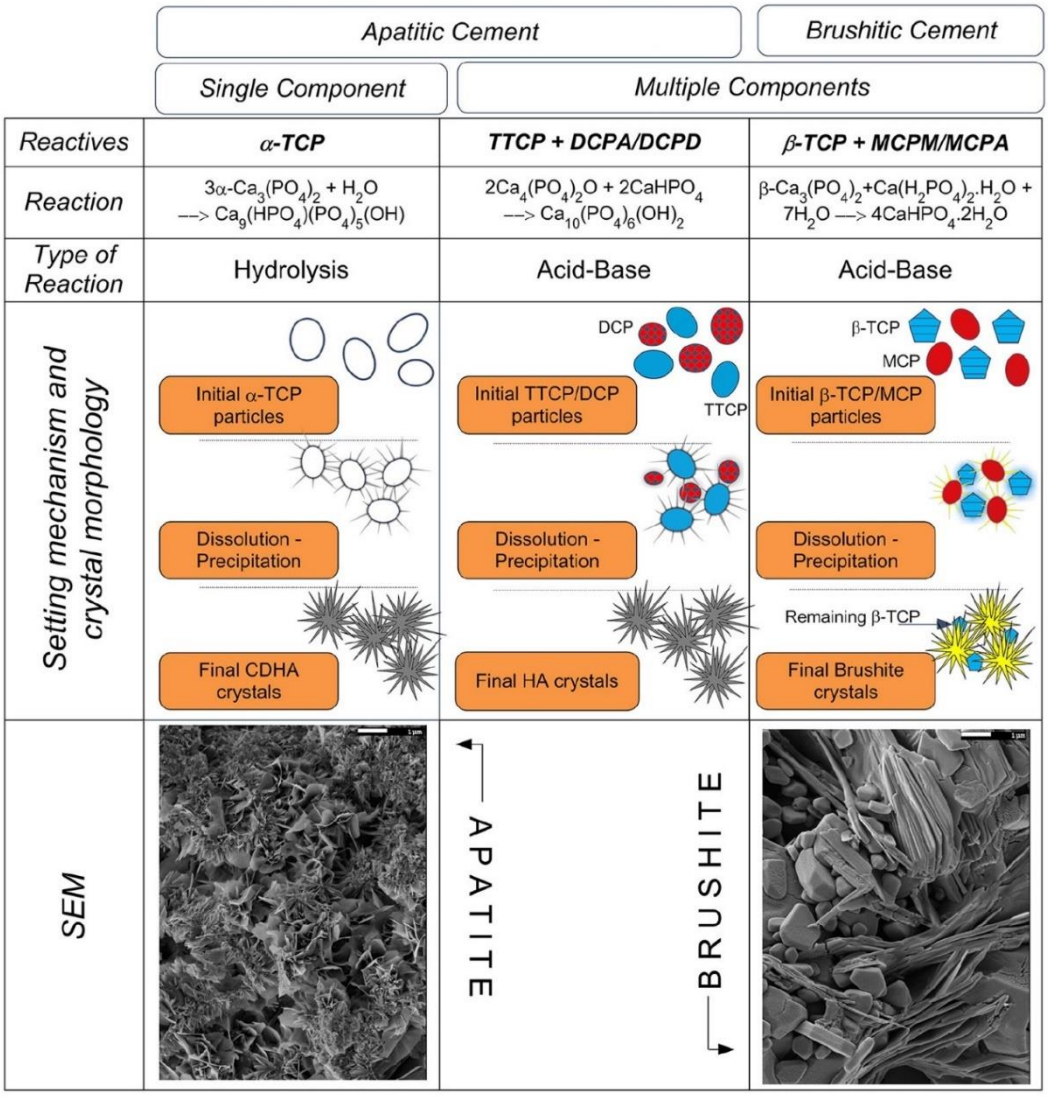



Figure 2.6: Summary of apatite and brushite production by hydrolysis and acid-base interactions of different reactives [31].

### 2.3.4 Calcium Phosphate/Calcium Sulfate Cement

Calcium phosphate-based bone cement are ideal bone-tissue materials due to their mechanical properties, three-dimensional structure with porosity for new bone formation, and biodegradability. The primary issue with apatitic cement is to optimize their degradation rate and bone ingrowth rate [38]. To optimize the new bone formation rate, porous structure is a necessity.

Calcium phosphate/calcium sulfate (CP/CS) cement are developed by mixing α-TCP with calcium sulfate hemihydrate (CSH) in an aqueous solution to create calcium-deficient hydroxyapatite (CDHAp) and resorbable calcium sulfate dihydrate (CSD) phases.

Setting reactions of α-TCP and CSH are shown in Equation. 1 and Equation. 2, respectively. In CP/CS cement; resorption of soluble CSD creates pores, and the apatitic CDHAp phase supports osteoconduction [39]. The compositional and ionic effect on the dissolution-precipitation mechanism of CP/CS cement are provided in Table 2.2.

Table 2.2: The effects of the amount of calcium sulfate dihydrate resorption and phosphate ion presence on the cement setting time [40].

| Explanation | Effect |
|---|---|
| CSD dissolution rapidly increases the supersaturation towards CDHAp in the mixing liquid. | The setting reaction starts earlier. Setting time decreases. |
| The dissolution of CSD increases the saturation of the mixing liquid towards $\alpha$-TCP, hence decreasing $\alpha$-TCP dissolution rate. | The setting reaction is slowed down. Setting rate decreases. |
| The presence of phosphate ions in the mixing solution increases its supersaturation towards CDHAp. | The setting reaction starts earlier. Setting time decreases. |
| The presence of phosphate ions in the mixing solution increases the saturation of the mixing liquid towards $\alpha$ -TCP, hence decreasing a-TCP dissolution rate. | The setting reaction is slowed down. Setting rate decreases. |
| The phosphate ions of the mixing liquid react with calcium ions stemming from CS dissolution to form CDHAp. This reaction releases hydronium ions that accelerate the setting reaction. | The setting rate increases. Setting time decreases. |

## 2.4 Calcium Phosphate-Based Composites

Ceramic/Polymer composites have been developed to optimize the mechanical properties, injectability, setting time, porosity, degradation rate, and osteoconduction of the materials made of single calcium phosphate-based ceramics. Polymers, materials with high toughness and flexibility, are the appropriate options to overcome the brittleness of ceramics [41].

Developed CaP/polymer-based materials are considered third-generation orthopedic biomaterials due to their improved properties than second-generation materials which are calcium phosphates, calcium sulfates, alumina, zirconia, polyurethanes, and polycaprolactone [42].

Natural bone's HAp/Collagen composite structure can be mimicked by polymer incorporations. The polymer phase of the composite is classified into two categories: synthetic and natural. Both synthetic and natural polymers have been used for certain applications depending on the needed clinical procedure.

Synthetic polymers in the composite structure are mainly polyethylene glycol (PEG), polymethyl methacrylate (PMMA), polyglycolic acid (PGA), poly-lactic-co-glycolic acid (PLGA), poly-l-lactic acid (PLLA) and polycaprolactone (PCL) [43, 44, 45]. Each reinforcement improves the mechanical properties. However, composites developed with synthetic polymers are either bioinert or able to release chemicals during the degradation process [45].

Reinforcement with natural polymers is the best option to mimic the natural bone's mineralized collagen fibril structure. Natural polymers used in bone-tissue engineering are silk, chitin, chitosan, hyaluronic acid, agarose, alginate, gelatin, and collagen.

Gelatin, a collagen derivative, is a completely resorbable natural polymer, unlike collagen [46]. It is advantageous because it degrades proteolytic, does not release acidic products, and does not express antigenicity [46, 47]. Gelatin is obtained by physical and chemical degradation of collagen or thermal denaturation.

Gelatin's similarity to the natural bone polymer collagen allows it to interact with the extracellular matrix and increase cell adhesion [48]. Among others, gelatin provides improved workability due to its physical cross-linking feature depending on the temperature. An aqueous solution of gelatin is in the sol state around 40 °C, and undergoes physical cross-linking when cooled down [49]. Chemical cross-linkers are only used for stabilizing gelatin in aqueous environments [46].

## 2.5 Calcium Phosphate-Based Microspheres

Calcium phosphates have been produced as granules and macroporous fast-resorbable blocks. However, shape and size control is crucial for cell adhesion. Microspheres ($\mu S$) with a diameter between 1 $\mu$m and 1000 $\mu m$ are suitable alternatives to blocks and granules with their spherical three-dimensional structure [50]. Spherical shape enhances the flowability and injectability into the irregularly shaped defects via a minimally invasive route [51].

Microspheres with tailorable size, shape, porosity, and surface roughness make them suitable for bone-tissue regeneration and drug delivery systems. Larger surface area and pores of the spherical shape increase the degradation rate, vascular ingrowth, and cell attachment [52].The fabrication processes of calcium phosphate ceramics strongly affect the geometrical and phasic characteristics.

Commonly used methods to fabricate CaP-based microspheres are based on the reagent and the media that particles are dispersed/aggregated. Reagents are divided into four types according to the amount of liquid they contain. The four types are solutions, slurries, pastes, and powders. Since the dispersion of fluid is easy, most methods are based on pastes, slurries, and solutions.

Production routes depend on the dispersion of reagents in a media. Dispersion media is either gas, liquid, or solid. CaP phase dispersed in gas and liquid form aerosol and emulsion, respectively. Dispersion of liquid in a solid phase is the lost wax method, and CaP phase acts as a mold in that procedure [53].

Solution-based methods are suitable for nano-sized particle production by spray drying, flame pyrolysis, precipitation, and precipitation-emulsification. Slurry-based methods are suitable for micro-sized particles due to the existing agglomerates in slurry. Droplet extrusion, emulsification, hydro-casting, and lost wax are the methods to produce microspherical slurry-based CaPs.

Pastes' rheological properties are difficult to adjust. Therefore, particles obtained by paste-based methods (sieve-shaking, spray granulation, extrusion-spheronization) are in the millimeter range. The powder-based method is plasma melting, which is the high-temperature melting of particles into spherical droplets. Particle size distribution depends on the powder size distribution in that process.

Spherical CaP particles contain liquid as a necessity to provide their shape. Therefore, consolidation is critical to prevent shape-deformation in the liquid phase. Methods used in consolidation are; drying, gelling, freezing, and crystallization. Consolidation methods are applied according to the production methods. For instance, drying, the simplest method, is not applicable in liquid-liquid dispersions [53]. In Figure 2.7, Production routes of spherical CaP formation methods are provided. Consolidated spheres require an additional stabilization step.

The methods used in the consolidation are also applicable in the stabilization step. Stabilization is achieved by sintering, hydrothermal conversion, and the addition of a binder. Gelification or cross-linking is involved in the stabilization of the binders [54]. Each process depends on the production method, composition, and aim of the production. Combinations of stabilization methods also possible. For instance, spherical CaP particles with binder incorporations are sintered in order to remove the binder [53]. In another approach, CaP spheres with binders are hydrothermally converted into HAp by the dissolution-precipitation reaction [54].

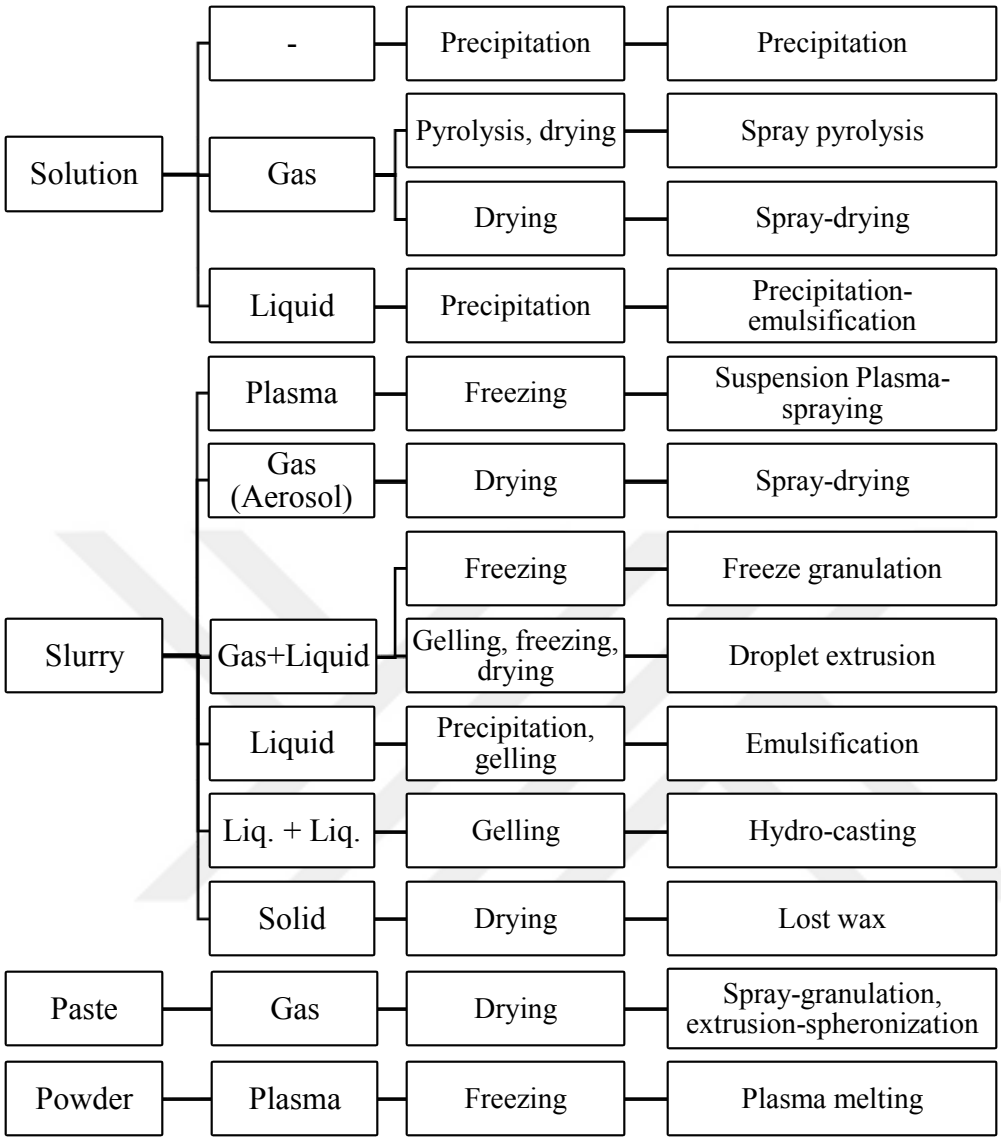



Figure 2.7: Schematic illustration of calcium-phosphate based microsphere production routes.

## 2.6 Emulsion-Based Processing

Emulsions are unstable dispersions that contain two immiscible liquids that are mixed with mechanical shear. Liquid droplets are dispersed in a continuous phase in emulsions [55]. Different types of emulsions are; oil-in-water (O/W), water-in-oil (W/O), water-in-oil-in-water (W/O/W) and oil-in-water-in-oil (O/W/O). Water and oil phases represent the hydrophilicity and hydrophobicity, respectively. There are several breakdown processes in emulsions such as creaming, sedimentation, flocculation, phase inversion, coalescence, and Ostwald ripening. Each breakdown process is illustrated in Figure 2.8.

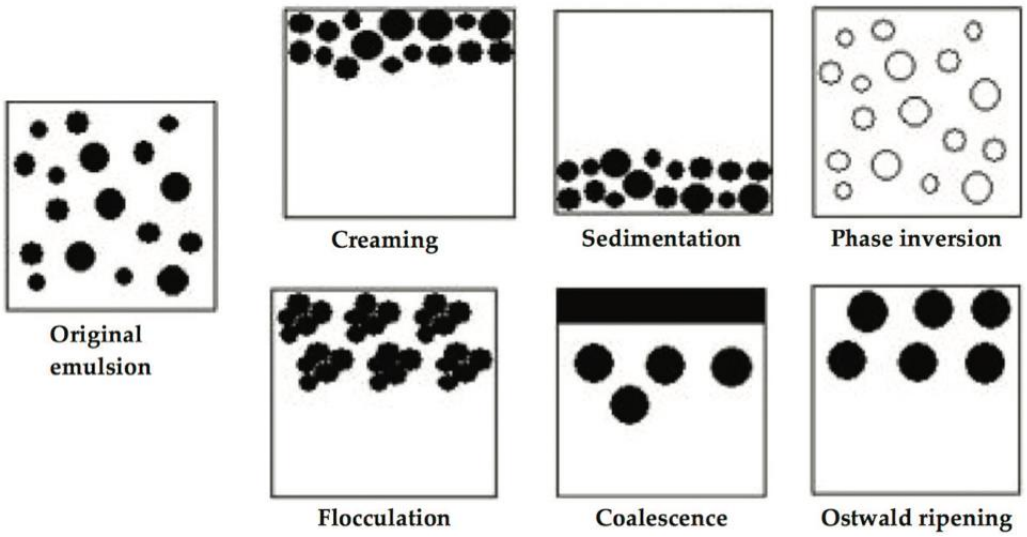



Figure 2.8: Schematic illustration of breakdown processes: creaming, flocculation, sedimentation, phase inversion, coalescence and Ostwald ripening. [56].

The emulsifiers, mostly referred to as surfactants, are commonly used in emulsion systems to disperse the system. Simple molecules, ions, polyelectrolytes, ionic surfactants, nonionic surfactants, mixed polymers, and solid particles are used as emulsifiers [57]. However, surfactants introduce complexities in the system due to their interactions with both disperse and continuous phases. Synthesis of solid particles and shaping of them through emulsion-based processing requires the removal of the surfactants. Therefore, surfactant-free emulsion systems are more appropriate for the preparation of solid products [58].

Production of calcium phosphate microspheres (CaP $\mu S$) by emulsion technique is possible by creating a water-in-oil (W/O) system. The hydrophilic phase in that system is CaP cement slurry [59]. The hydrophilic calcium phosphate phase is mechanically dispersed in the oil (hydrophobic) phase in the emulsion. to produce calcium phosphate microspheres, the hydrophilic calcium phosphate phase is mechanically dispersed in the oil (hydrophobic) phase in the emulsion. The precipitated microspheres are then separated from the continuous oil phase.

# CHAPTER 3

# MATERIALS AND METHODS

The main constituent of microspheres, $\alpha$-tricalcium phosphate ($\alpha$TCP, $\alpha$-$Ca_3(PO_4)_2$) powders used in this thesis was synthesized via the solid state reaction. Solid state synthesis of phase pure $\alpha$-tricalcium phosphate ($\alpha$-TCP, $\alpha$-$Ca_3(PO_4)_2$), production of composite ($\alpha$-TCP/Alginate, $\alpha$-TCP/Gelatin, and $\alpha$-TCP/CSH/Gelatin) microspheres and their hydration products are represented in this chapter. Compositions of each material in the composites and tested emulsion parameters are described in detail in relevant sections.

## 3.1 Materials

Calcium carbonate ($CaCO_3$, reagent grade, Merck, Germany) and phosphoric acid ($H_3PO_4$, reagent grade, 85%, Merck, Germany) were used as the calcium and phosphate sources in solid-state synthesis of $\alpha$-TCP powders. Primarily, monetite ($CaHPO_4$, dicalcium phosphate anhydrous, DCPA) was synthesized chemically to produce $\alpha$-TCP. Stoichiometric amounts of monetite and $CaCO_3$ were subsequently fired at 1200 °C. Aqueous solutions of sodium alginate ($(C_6H_7NaO_6)_n$, Sigma Aldrich, USA) and gelatin (type A, Sigma Aldrich, USA) were used to produce $\alpha$-TCP/Alginate, $\alpha$-TCP/Gelatin, $\alpha$-TCP/CSH/Gelatin) composites. Calcium sulfate hemihydrate ($CaSO_4 \cdot {}^1/_2H_2O$, Sigma-Aldrich, USA) was used in $\alpha$-TCP/CSH composites with different compositions. Calcium chloride (anhydrous, reagent grade, $CaCl_2$, Supelco, USA) was used to cross-link the Na-Alginate. Glutaraldehyde solution (Grade 1, 25% in $H_2O$, Sigma-Aldrich, USA) was used to cross-link gelatin. Acetone ($(CH_3)_2CO$, Sigma-Aldrich, USA) was used for the washing procedure. DI water and phosphate buffer (Fluka, Switzerland) solution (PBS) were used to hydrate the obtained products. Sunflower oil was used as a continuous phase in the emulsion.

## 3.2 Methods

### 3.2.1 α-TCP Synthesis

Monetite, one of the precursors of α-TCP, was chemically synthesized. First, 20 g of $CaCO_3$ was calcined at 1010 °C for 2 h. Produced 11.2 g of CaO was then hydrated with 200 mL excess DI water for 1h while stirring. 23.03 g (approximately 13.55 mL) of $H_3PO_4$ was added to the system to keep the molar ratio 1:1 with the hydration product $Ca(OH)_2$. The temperature was set to 60 °C and stirred for 1.5 h to obtain monetite ($CaHPO_4$). The product slurry was vacuum filtered and dried at 70 °C for 1 day. High-temperature solid-state reaction of $CaCO_3$ and chemically synthesized $CaHPO_4$ was conducted to produce α-TCP. Mentioned reaction formula is demonstrated in Equation 6.

$$2CaHPO_{4(s)} + CaCO_{3(s)} \rightarrow Ca_3(PO_4)_{2(s)} + CO_{2(g)} + H_2O_{(g)} \quad (6)$$

2:1 molar ratio of $CaHPO_4$ and $CaCO_3$ were mixed in a Nalgene container with 100 mL acetone and 15 zirconia balls (10 mm diameter) for 2 h to mix the two compositions homogenously. Turbula mixer (Model T2F, System Schatz, Switzerland) was used for mixing. The homogenized mixture was dried in open-air conditions for 1 day to evaporate acetone from the mixture. After the evaporation, the mixture was fired at 1200 °C for 2 h in an alumina crucible. Obtained hot mass after 2 h of firing was immediately air-quenched to prevent phase transformation. Quenched product was milled in a Nalgene bottle with 15 zirconia calls and 100 mL acetone for 3h. Synthesis process of $\alpha$-TCP is shown in Figure 3.1.

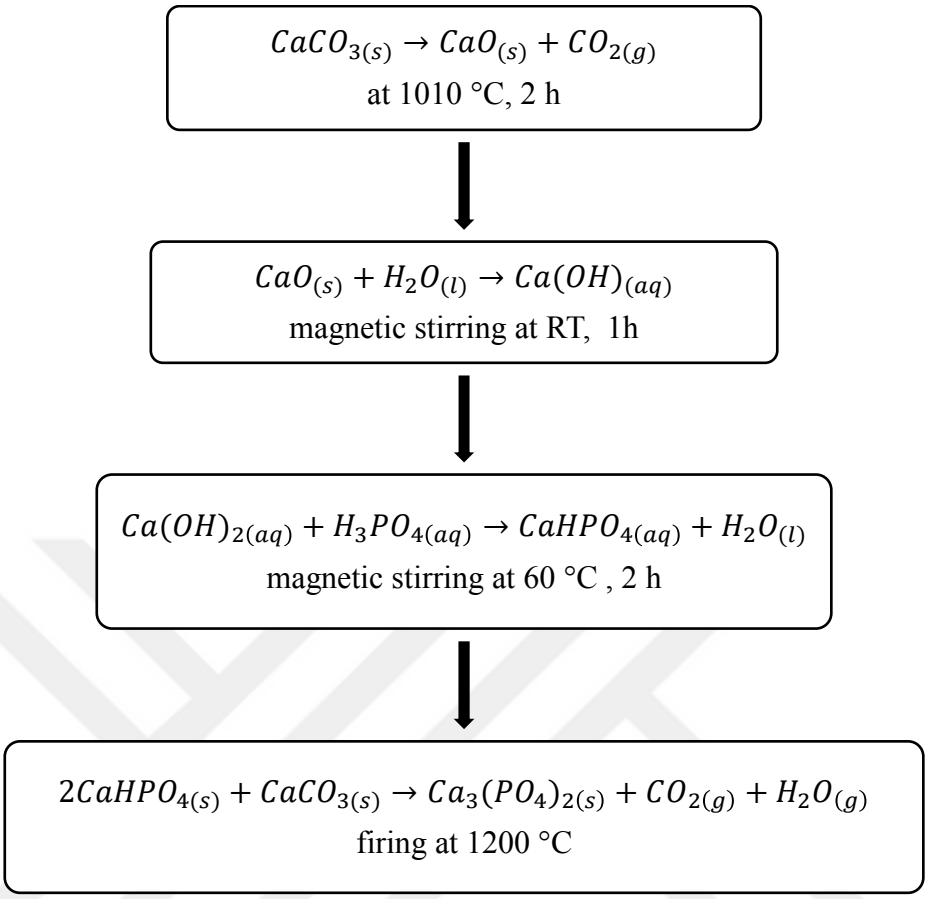



Figure 3.1: Flow chart of α-TCP synthesis procedure.

### 3.2.2 Production of Calcium Phosphate-Based Microspheres

Formation of calcium phosphate-based microspheres was conducted by six steps: mixing α-TCP powder or α-TCP/CSH hybrid with an organic (alginate or gelatin) binder, dispersion of the α-TCP-based slurry in a continuous sunflower phase, gelling or cross-linking of the organic binder, separation of the oil phase, washing and drying. Same 100 mL flat-bottom borosilicate glass container, with the same amount of sunflower oil as 60 mL and the same 3 cm PTFE stirring bar was used in all emulsions. A schematic illustration of the mentioned process is provided in Figure 3.2. Produced liquid microspheres in each case were washed and dried by the same

methods. After ending the dispersion by magnetic stirring, sediments were separated from the oil phase by adding DI water into the emulsion. After the separation of the oil phase, 20 mL of acetone was added to dehydrate the microspheres. Spherical aggregates were collected and washed 5 times with acetone for removal of any residual oil that may remain on the particles and further dehydration. Washed particles were air-dried overnight.

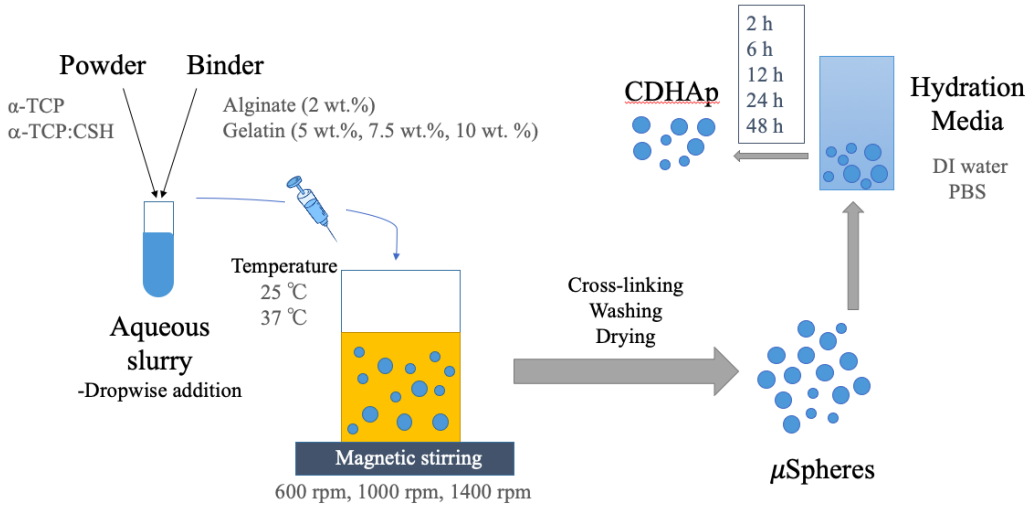



Figure 3.2: Schematic illustration of emulsion-based processing of TCP microspheres.

#### 3.2.2.1 α-TCP/Alginate Microspheres

Alginate solution was prepared by dissolving 2 g of sodium alginate powder in 100 mL DI water at room temperature to solve with 2 wt.% concentration. 4 mL of the solution was mixed with 2 g of previously synthesized α-TCP. The powder-liquid ratio was set to 1:2 to obtain a well-dispersed slurry. Prepared α-TCP/Alginate slurry was added into stirring oil dropwise by a 5 mL syringe. After the slurry was dispersed in the emulsion for 15 minutes under continuous stirring, 0.2 M $CaCl_2$ solution was introduced into the stirring emulsion drop by drop to cross-link the organic alginate phase. The stirring speed was gradually decreased after 10 minutes of additional continuous stirring. α-TCP/Alginate particles were collected, washed, and dried.

Cross-linking of sodium alginate is shown in Equation 7.

$$2Ca_6O_7NaO_6 + CaCl_2 \rightarrow 2NaCl + C_{12}H_{14}CaO_{12} \quad (7)$$

#### 3.2.2.2 α-TCP/Gelatin Microspheres

Gelatin solutions of different concentrations were prepared by dissolving gelatin in DI water at 40 °C under continuous magnetic stirring for 15 minutes. 4 mL of each concentration was mixed with 2 g α-TCP to keep the powder-liquid ratio constant. The ratio was decided according to the viscosity of the most concentrated gelatin solution. Prepared α-TCP/Gelatin slurries were introduced into the stirring oil drop by drop with a 5 mL syringe at different stirring speeds and temperatures. After the slurry was dispersed in the oil, the emulsion was cooled down to ~5 °C in an ice water bath under continuous stirring for additional 15 minutes for gelling. The stirring speed was gradually decreased, and the emulsion was placed in an iced-water bath for sedimentation. The oil phase was removed by adding 4 °C water.

After removing the oil phase, produced microspheres were collected washed, and dried. Dry α-TCP/Gelatin (α-TCP/G) microspheres were cross-linked with 0.5%

glutaraldehyde solution for 1 h. Cross-linked microspheres were collected washed, and dried with the same method. By using this method, 18 α-TCP/Gelatin samples were prepared. Details of microsphere production are provided in Table 3.1

Table 3.1: Detailed preparation parameters of α-TCP/Gelatin (α-TCP/G) microspheres.

| **Temperature (°C)** | **Gelatin Concentration** | **Stirring speed (rpm)** | **Sample ID** |
|---|---|---|---|
| 25 | 10 wt.% | 600 | 1 |
| | | 1000 | 2 |
| | | 1400 | 3 |
| | 7.5 wt.% | 600 | 4 |
| | | 1000 | 5 |
| | | 1400 | 6 |
| | | 600 | 7 |
| | | 1000 | 8 |
| | | 1400 | 9 |
| 37 | | 600 | 10 |
| | | 1000 | 11 |
| | | 1400 | 12 |
| | 5 wt.% | 600 | 13 |
| | | 1000 | 14 |
| | | 1400 | 15 |
| | | 600 | 16 |
| | | 1000 | 17 |
| | | 1400 | 18 |

#### 3.2.2.3 α-TCP/CSH/Gelatin Microspheres

α-TCP/CSH hybrid powders were produced by mixing α-TCP powders with calcium sulfate hemihydrate powders (CSH, $CaSO_4 \cdot {}^1/_2H_2O$) in different compositions. Powders in acetone media were mixed by using Turbula mixer for 1h. The wet mixture was air-dried overnight to evaporate acetone. Dry powders were mixed with 5 wt.% gelatin solution to obtain a slurry. α-TCP/CSH/G slurry was dispersed in sunflower oil by magnetic stirring at 1000 rpm. Gelling, separation, drying, cross-linking, and washing steps were conducted by following the same α-TCP/G microsphere production methods. α-TCP/CSH compositions, used powder amounts, and their abbreviations are provided in Table 3.2.

Table 3.2: Detailed compositional information of α-TCP/CSH microspheres.

| Abbreviation | CSH | α-TCP | α-TCP/CSH | Gelatin Solution | L:P |
|---|---|---|---|---|---|
| CS10 | 1 g | 9 g | 9:1 | 20 mL | 2:1 |
| CS25 | 2.5 g | 7.5 g | 3:1 | 20 mL | 2:1 |

#### 3.2.2.4 Post-Processing Treatments of Calcium Phosphate-Based Microspheres

Microspheres with α-TCP/G and α-TCP/CSH/G compositions were immersed in DI water and phosphate buffer solution (PBS) at 37 °C. Samples were collected at various time intervals (2 h, 6 h, 12 h, 24 h, 48 h). Collected samples were crushed with alumina mortar and pestle for further analysis. PBS was prepared at 25 °C by dissolving 34 g of phosphate buffer in 1 L DI water.

### 3.2.3 Material Characterization

#### 3.2.3.1 Phase Identification: X-ray Diffraction Analysis (XRD)

The X-ray diffraction analyses were performed with the diffractometer (Rigaku, Germany) equipped with x-ray tube with CuKα radiation of λ=1.5418 Å that operated at 40 kV and 30 mA. The XRD analyses were performed with a scanning rate of 2°/min. The synthesis product monetite was scanned at 2θ of 20°-50°. The synthesis product α-TCP, α-TCP/Gelatin microspheres, and the hydration products were scanned at 2θ of 20°-40°. The microspheres including calcium sulfate phase (TCP/CS) and their hydration products were scanned at 2θ of 10°-40°. The phases were identified by comparing with the JCPDS cards of monetite (JCPDS PDF 00-09-080), α-TCP (JCPDS PDF 00-09-348), CDHAp (JCPDS PDF 00-009-0432), CSH (JCPDS PDF 00-09-080) and CSD (JCDPS PDF 00-09-345).

#### 3.2.3.2 Chemical Analysis: Fourier Transformed Infrared Spectroscopy

Attenuated total reflectance-Fourier transform infrared spectroscopy (ATR-FTIR) analyses were performed with FTIR Frontier spectrometer (Perkin Elmer, USA). The FTIR spectra were collected between 400-4000 wavenumbers ($cm^{-1}$). The synthesis products, polymeric additives, cross-linking of the polymeric additives, and hydration products have been investigated using FTIR.

#### 3.2.3.3 Viscosity Measurements

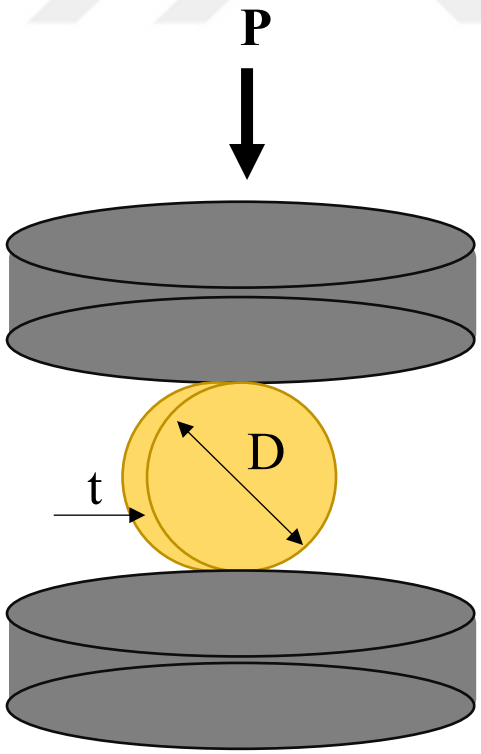
The viscosity analyses of oil phase of the emulsion at different temperatures were performed by using Brookfield DV-E viscometer. The viscosities were measured in a 250 mL beaker with the appropriate accessory apparatus of the instrument.

#### 3.2.3.4 Microstructural Investigation: Scanning Electron Microscopy (SEM)

The microstructure of the solid-state intermediate calcium phosphate powders and end synthesis products, as well as-prepared TCP/Gelatin microspheres and TCP/CS microspheres and the hydrated microspheres were investigated by a FEI Quanta 400F model field emission scanning electron microscope. The SEM examinations were performed after coating with conductive gold layer.

#### 3.2.3.5 Mechanical Test: Diametral Compression Test

The mechanical properties of the TCP/Gelatin, TCP/CS, and their hydration products were determined using diametral compression test using coin shaped pellet analogs of the respective microsphere formulations. The tests were performed using Instron 5565A 5 kN at room temperature.



The fracture strength of the samples were determined by the following formula;

$$\sigma = \frac{2P}{\pi Dt}$$

where;

P = maximum compressive load (N),

D = diameter (cm),

t = thickness (cm).

# CHAPTER 4

# RESULTS AND DISCUSSION.

## 4.1 Characterization of Synthesis Products

In this chapter, the characterization of solid-state reaction product α-TCP and its chemically synthesized precursor monetite are presented. Phase analysis of each product was performed by XRD in order to ensure the phase characteristics of synthesis products monetite and α-TCP. The chemical characteristics of synthesis products were analyzed by FTIR. Microstructural physical features were investigated by SEM.

### 4.1.1 Characterization of Monetite

α-TCP is the solid state reaction product between monetite ($CaHPO_4$) and $CaCO_3$ as described in the Chapter 3. Therefore, it is an undeniable fact that the characterization of chemical synthesis product monetite is substantial. The diffractogram in Figure 4.1 shows the XRD pattern of produced powder that completely matches with monetite phase with JCPDS card no 09-080.

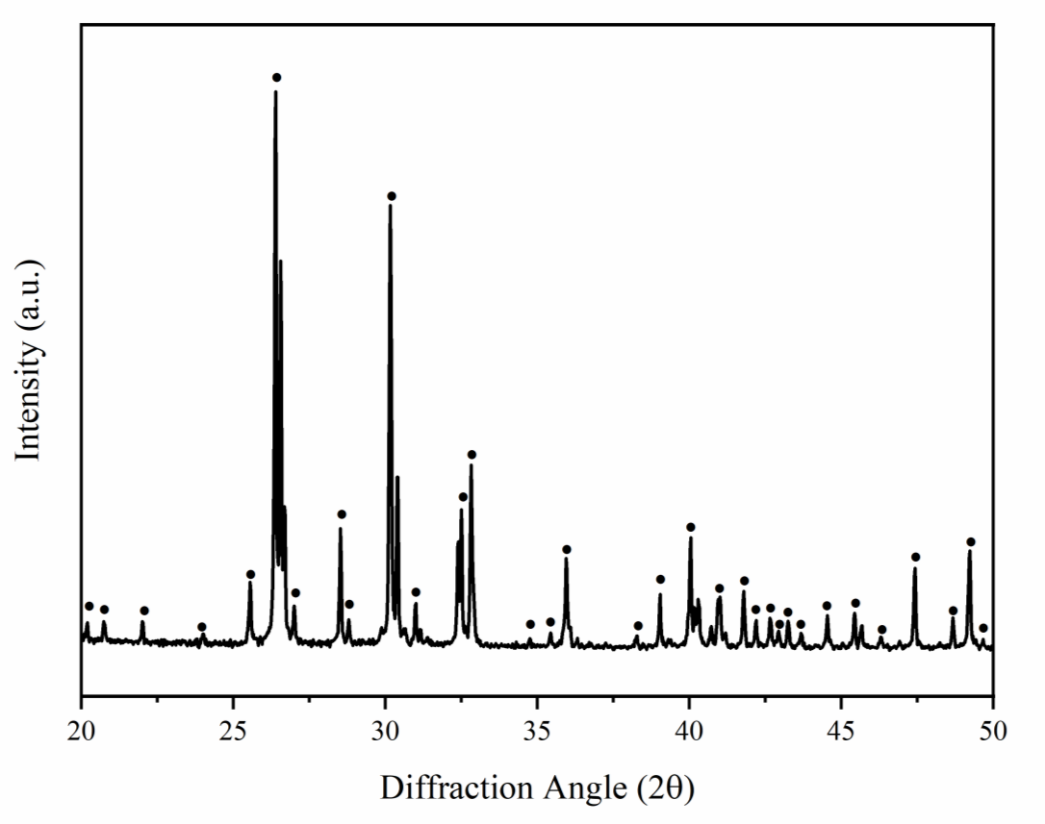



Figure 4.1: XRD diffractogram of monetite matching JCPDS card no 09-080

FT-IR spectrum of monetite is shown in Figure 4.2. According to the literature, the bands at 523 $cm^{-1}$, 559 $cm^{-1}$, 993 $cm^{-1}$, 1058 $cm^{-1}$, and 1124 $cm^{-1}$ are related with the P-O bending and stretching modes. The band at 888 $cm^{-1}$ is related with P-OH stretching mode. The 1348 $cm^{-1}$ and 1396 $cm^{-1}$ are O-H bending modes, and the1644 $cm^{-1}$ is the O-H bending and rotation of residual free water [60, 61]. The SEM micrograph in Figure 4.3 shows the microstructural features of monetite. The monetite crystals exhibit a defined, irregularly granulated morphology.

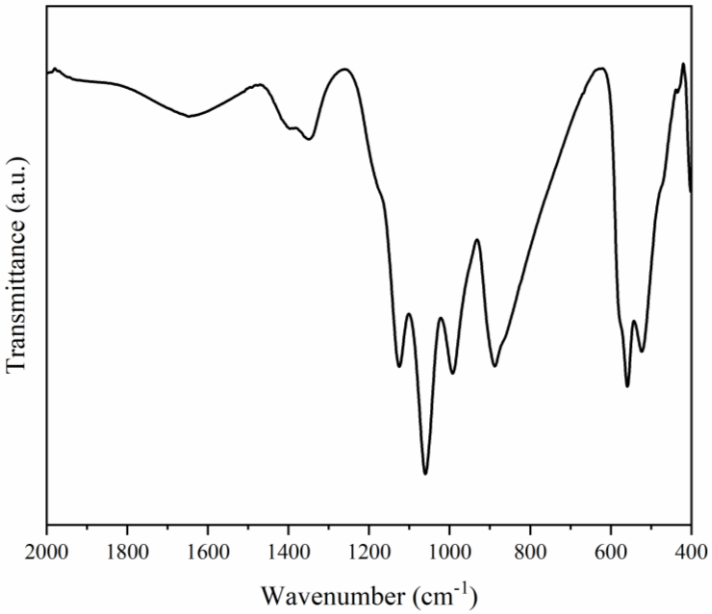



Figure 4.2: FTIR spectrum of monetite.

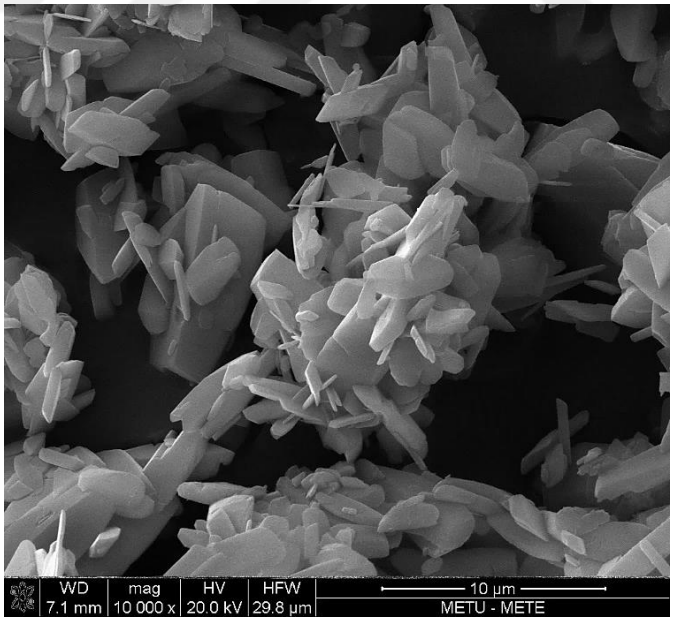



Figure 4.3: SEM micrograph of monetite ($CaHPO_4$).

### 4.1.2 Characterization of α-TCP

Monetite powder was mixed with $CaCO_3$ and co-fired at 1200º C for 2 h and, the product was air quenched immediately to obtain phase pure α-TCP. The XRD diffractogram of the synthesis product is given in Figure 4.4 that completely matches with the phase pure $\alpha$-TCP with JCPDS card no 09-348. The XRD data reveals that air-quenching was effective since transformation of metastable α-TCP phase to thermodynamically stable polymorph, i.e. β-TCP did not occur. Additionally HAp phase that can be formed potentially due to environmental vapor was not observed. Phase pure α-TCP production was substantial since the transformation between phases can affect the reactivity. α-TCP is the least stable phase at room temperature, therefore setting reaction (via hydration by water uptake) of α-TCP in an aqueous media is superior to other TCP polymorphs.

The chemical analysis of α-TCP ($Ca_3(PO_4)$) was performed by using FTIR. In Figure 4.5 , transmittance spectrum of α-TCP powders in the range of 2000-500 $cm^{-1}$ is shown. The $PO_4$ structural group chemical information based on two phosphate bands and their details are shown in the data. The bands between 500 $cm^{-1}$ and 700 $cm^{-1}$ are antisymmetric bending mode of P–O, the bands between 800 $cm^{-1}$ and 1100 $cm^{-1}$ are symmetric and antisymmetric stretching modes of P–O. The FTIR data does not provide specific information about α-TCP, but it is a useful reference data to understand/reveal and chemical changes that can occur upon mixing with polymer in forming microspheres or when it is hydrated.

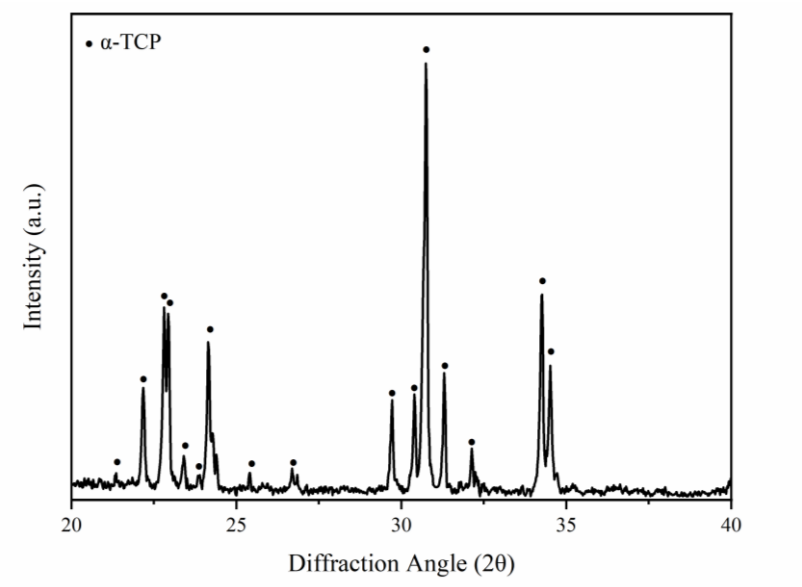



Figure 4.4: XRD diffractogram of α-TCP that matches with JCPDS card no 09-348.

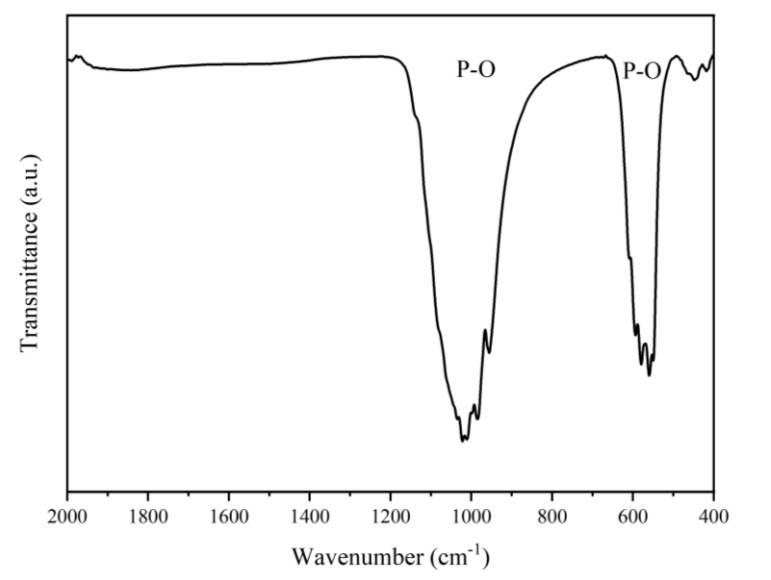



Figure 4.5: FTIR spectrum of α-TCP.

The typical morphology and characteristic microstructural features of α-TCP is shown in Figure 4.6. The SEM micrograph shows a smooth, partially fused, and irregularly granulated morphology typical to ceramic powder produced by solid state reaction. It is hard define a distinct particle size due to partial fusion, but it can be approximated to an average particle size of 3-5±1 μm according to SEM data.

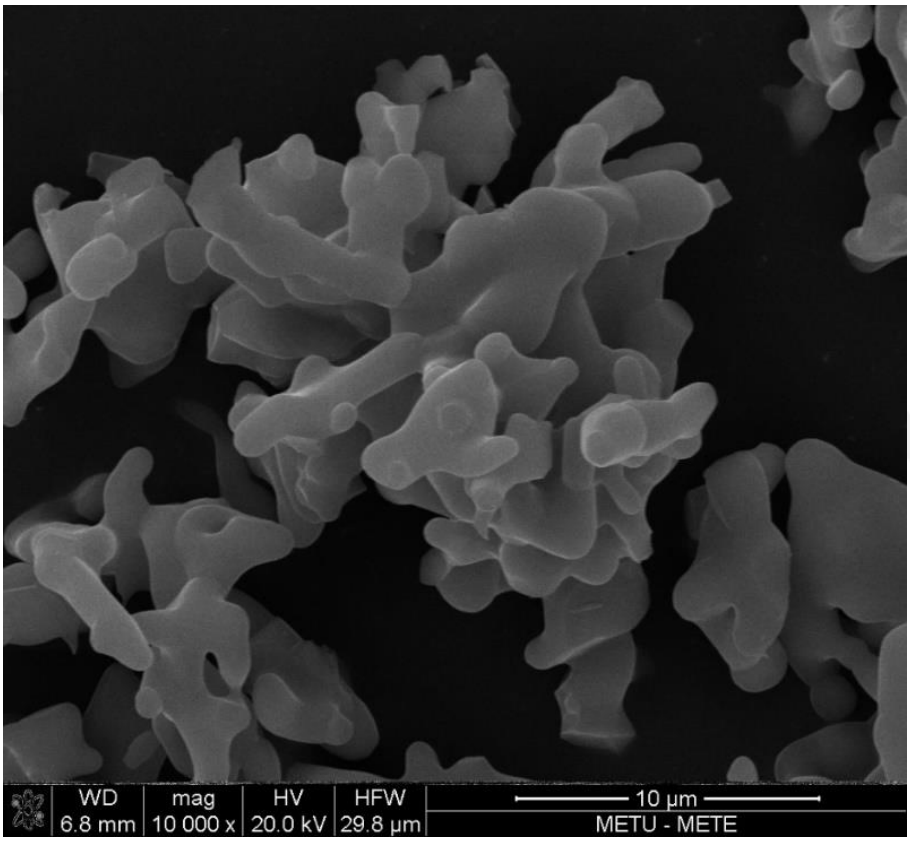



Figure 4.6: SEM micrograph of α-TCP.

## 4.2 Characterization and Properties of α-TCP/Polymer Microspheres

The synthesized α-TCP powders were mixed with binder solutions to obtain a slurry as previously stated in Chapter 3. The binder solutions were prepared with different polymers (binders) and compositions. The effects of binder solution formulations (2 wt.% sodium alginate, 5 wt.% gelatin, 7.5 wt.% gelatin, and 10 wt.% gelatin) on chemical composition, microsphere formation and shape/morphology of microspheres were investigated.

### 4.2.1 Characterization of α-TCP/Alginate Microspheres

The first binder in microsphere formation studies was alginate. α-TCP-based microspheres were prepared with 2 wt.% sodium alginate solution (Na-Alginate) which were cross-linked to calcium alginate (Ca-Alginate) in the emulsion. Cross-linked microspheres were then dried and examined.

The chemical composition of the sodium alginate solution and cross-linking effect on the α-TCP/Alginate microspheres with $CaCl_2$ were examined by using FTIR spectroscopy. The FTIR spectra of pure α-TCP, alginate solution (Na-Alginate), α-TCP/Alginate microspheres are shown in Figure 4.7.

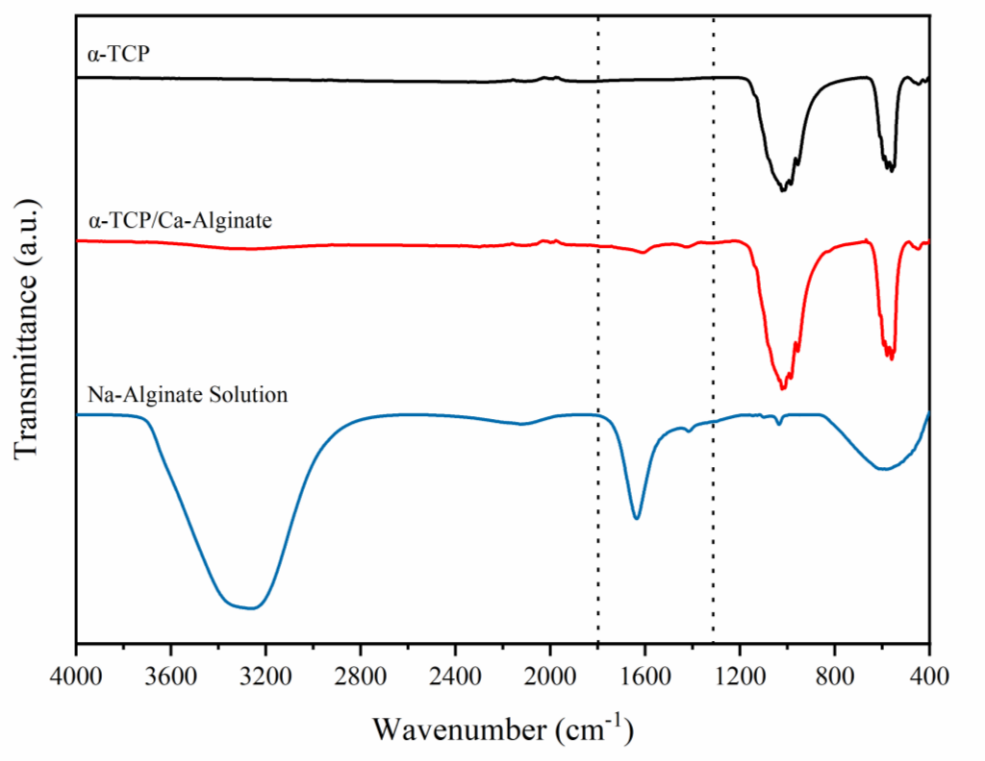



Figure 4.7: FTIR spectra of Na-Alginate solution, cross-linked α-TCP/Ca-Alginate microspheres, and pure α-TCP.

The solution band between the 2800 $cm^{-1}$ and 3700 $cm^{-1}$ wavenumbers corresponds to the O–H stretching of loosely bound water in solution. The bands observed in the solution at 1635 $cm^{-1}$ and 1413 $cm^{-1}$ wavenumbers are the asymmetric and symmetric stretching modes of carboxylate ion [62, 63]. The shift from 1635 $cm^{-1}$ to 1610 $cm^{-1}$, and 1413 $cm^{-1}$ to 1421 $cm^{-1}$ and intensity decrease were observed in α-TCP/Alginate. The shifts to different wavenumbers of carboxyl ($–COO^-$) groups indicates ionic binding between $CaCl_2$ and alginate [64]. Therefore, cross-linking of sodium alginate to calcium alginate occurred to a certain extent.

The microspheres formed with sodium-alginate were cross-linked by adding $CaCl_2$ into the emulsion under continuous stirring. Therefore, cross-linking was not controlled directly and precisely. This leads to certain problems in terms of microsphere formation as revealed by the SEM investigation. The SEM micrograph indicating the morphology of α-TCP/Alginate microspheres is shown in Figure 4.8. The cross-linked microspheres exhibited structural defects as can be noticed from these images; such as shape distortion, agglomeration, and integration into irregular large forms. Alginate found to be not an effective and proper binding agent for consolidating α-TCP particles to sphere form. No further study was performed using alginate binder.

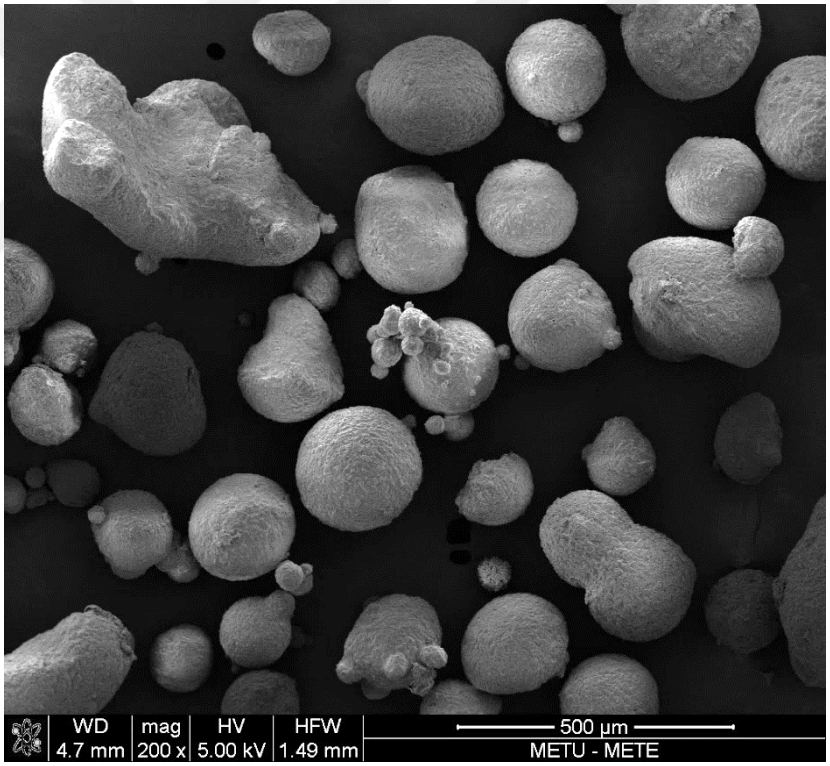



Figure 4.8: SEM microgpraph of $\alpha$ -TCP/Alginate particles.

### 4.2.2 Characterization of α-TCP/Gelatin Microspheres

After alginate-based trials, α-TCP/Gelatin microspheres were prepared at different gelatin concentrations (containing 5.0, 7.5, 10.0 wt.% gelatin), and varying microemulsion parameters such as stirring speed, and oil temperature. The chemical analysis/changes during gelatin: α-TCP powder integration and cross-linking of different concentrations was conducted by FTIR. The morphologies of the final microspheres obtained with different emulsion process parameters were examined with SEM.

The α-TCP/Gelatin microspheres were prepared by mixing gelatin solutions with α-TCP powders. The abbreviations of α-TCP/Gelatin microspheres prepared with 5, 7.5, and 10 wt.% gelatin concentrations are TCP/G-5, TCP/G-7.5, and TCP/G-10, respectively.

This time not an *in-situ* cross-linking was performed and the final microspheres of emulsion process were cross-linked afterwards after removing partially matured microspheres from the emulsion system. The FTIR spectra showing the chemical structure of α-TCP powders, gelatin solution, and gelatin incorporated α-TCP mixtures (at different gelatin amounts) before cross-linking are shown in Figure 4.9.

The band between 2800 $cm^{-1}$ and 3750 $cm^{-1}$ that is observed only in gelatin solution (GS) indicates the O–H stretching mode of water. The band between 1580 $cm^{-1}$ and 1750 $cm^{-1}$ corresponds to C=O and C–N stretching vibration of the Amide I band. The Amide II band is in the range of 1560-1335 $cm^{-1}$, and corresponds to the bending vibration of N-H and stretching vibrations of C–N groups [65, 66]. Therefore, the bands of $\alpha$-TCP/Gelatin at 1635 $cm^{-1}$ is the Amide I band, while bands at 1555 $cm^{-1}$ and 1460 $cm^{-1}$ are Amide II bands. The peak positions of Amide I and Amide II are essential to investigate the chemical cross-linking of gelatin. The FTIR spectra of cross-linked α-TCP/Gelatin microspheres with different concentrations of gelatin are shown in Figure 4.10.

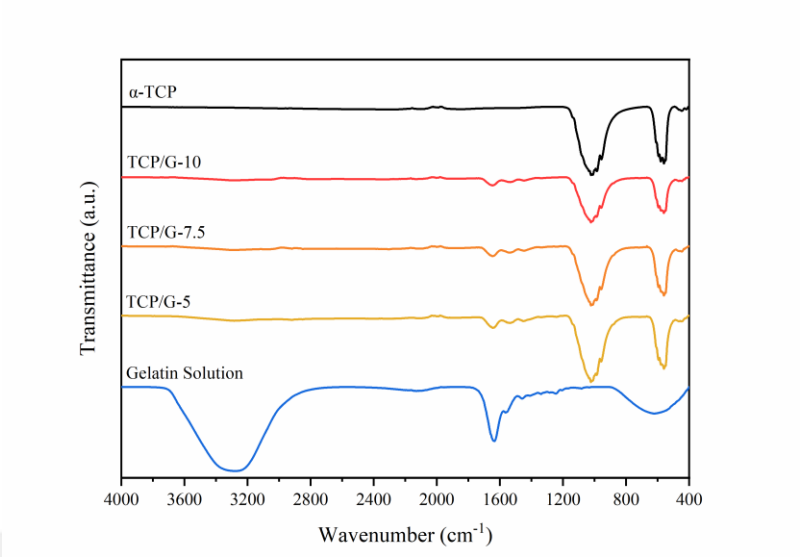



Figure 4.9: FTIR spectra of α-TCP, TCP/G-5, TCP/G-7.5, TCP/G-10, and gelatin solution.

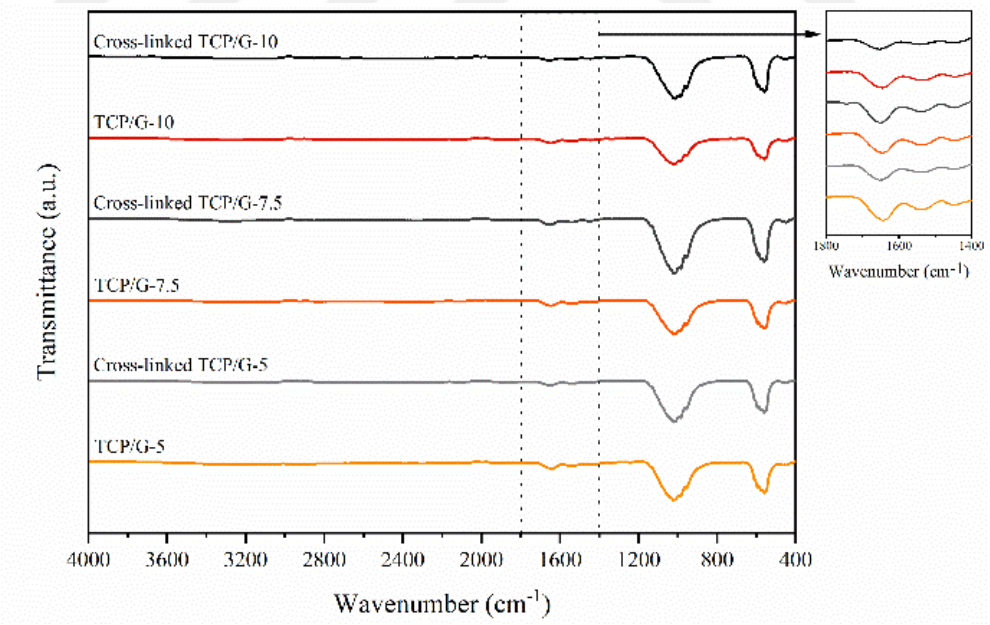



Figure 4.10: FTIR spectra of TCP/G-5, TCP/G-7.5, TCP/G-10, and cross-linked TCP/G-5, cross-linked TCP/G-7.5, and cross-linked TCP/G-10.

The slight shifts of Amide I and Amide II bands corresponds to intermolecular interactions between amino-groups of gelatin and glutaraldehyde. Each gelatin composition (5, 7.5, and 10 wt. %) showed minor shifts in the amide bands. Amide I band of each composition shifted to smaller wavenumbers. The Amide I band of TCP/G-5, TCP/G-7.5, and TCP/G-10 shifted from 1644 $cm^{-1}$ to 1651 $cm^{-1}$, 1652 $cm^{-1}$ to 1644 $cm^{-1}$, and 1646 $cm^{-1}$ to 1656 $cm^{-1}$, respectively. Therefore, cross-linking with glutaraldehyde was effective on each concentration. After cross-linking, color changes (slightly towards yellow) were observed on microspheres and shown in Figure 4.11. The highest gelatin concentration exhibited the darkest color, and the lowest gelatin concentration exhibited the lightest color. The observed color changes were due to the aldimine (C=N) linkage between gelatin and glutaraldehyde [67].

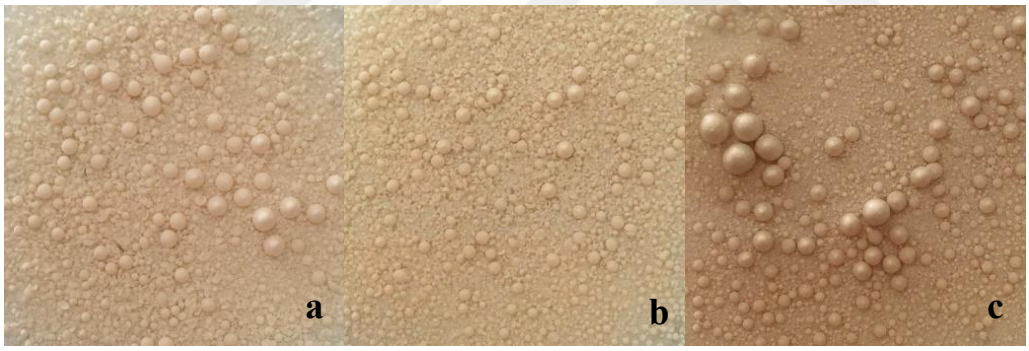



Figure 4.11: Color changes on a) TCP/G-5, b) TCP/G-7.5, and c) TCP/G-10 after cross-linking.

TCP/Gelatin microspheres prepared with each concentration exhibited well-defined spherical morphology due to effective cross-linking, unlike TCP/Alginate microspheres. The SEM micrographs showing the spherical shapes without any shape deformation are shown in Figure 4.12. The spherical shape was preserved regardless of the gelatin amount. Each gelatin concentration provided a well-defined morphology.

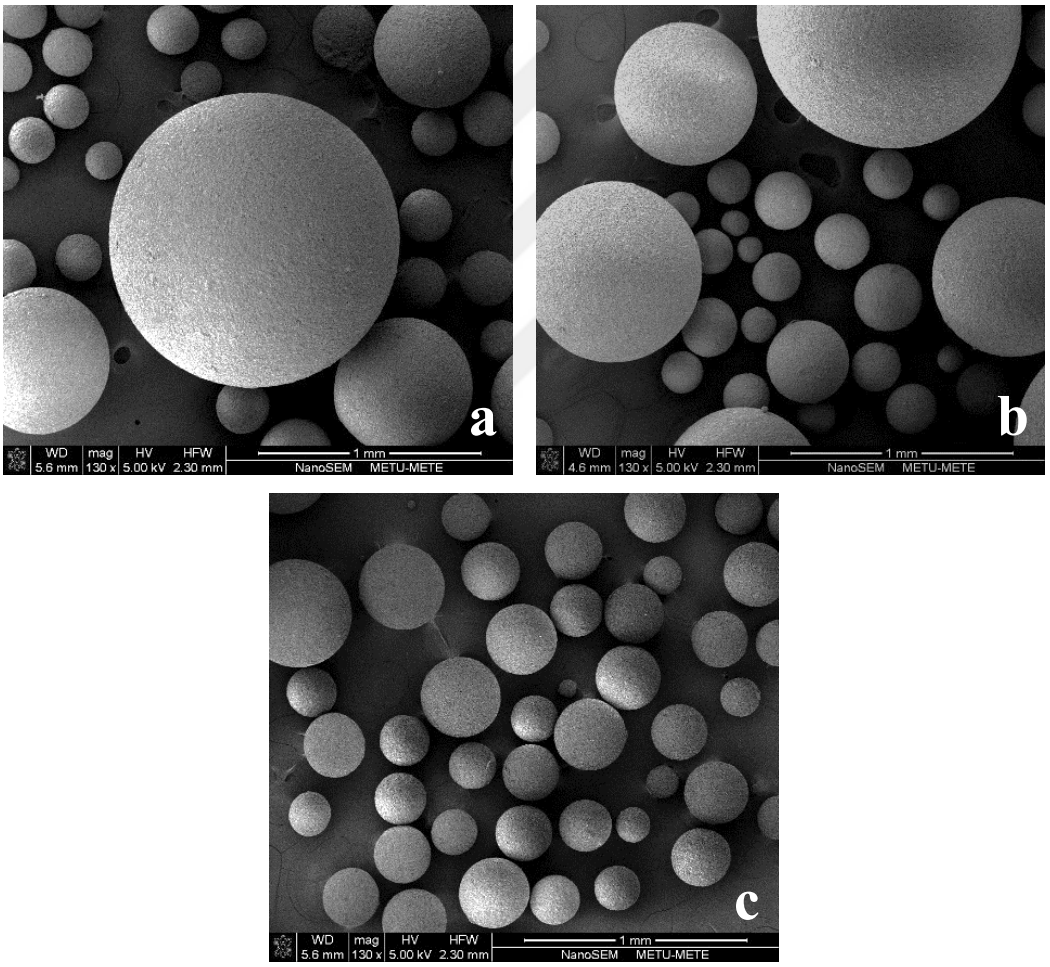



Figure 4.12: SEM micrographs of a) TCP/G-10, b) TCP/G-7.5, and TCP/G-5.

#### 4.2.2.1 Effect of Emulsion Parameters on Microsphere Size/Morphology

The morphological changes on TCP/Gelatin microspheres at different stirring rates (600 rpm, 1000 rpm, and 1400 rpm). were examined by SEM analysis. The SEM micrographs shown in Figure 4.13 indicate the size distribution of the TCP/Gelatin microspheres prepared at 600 rpm, 1000 rpm, and 1400 rpm stirring rates at 25 °C.

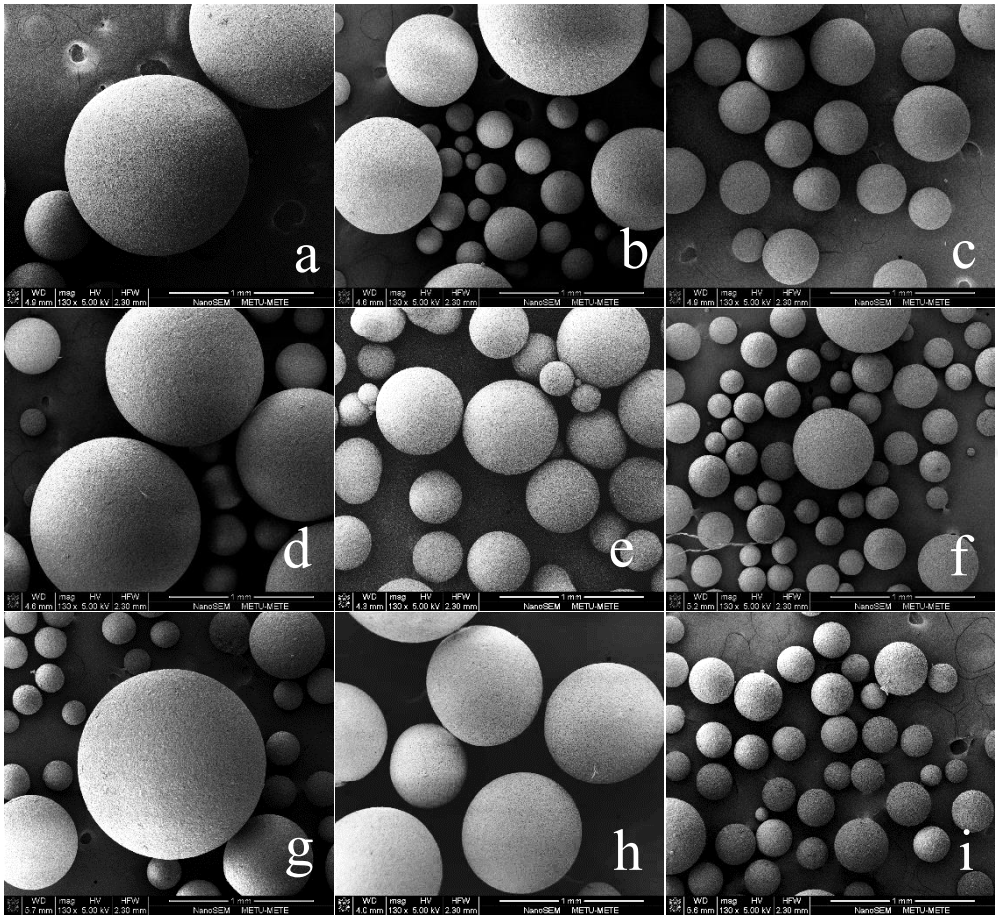



Figure 4.13: SEM migrographs of a)TCP/G-5 stirred at 600 rpm, b)TCP/G-5 stirred at 1000 rpm, c)TCP/G-5 stirred at 1400 rpm, d)TCP/G-7.5 stirred at 600 rpm, e) TCP/G-7.5 stirred at 1000 rpm, f) TCP/G-7.5 stirred at 1400 rpm, g)TCP/G-10 stirred at 600 rpm, h)TCP/G-7.5 stirred at 1000 rpm, and i)TCP/G-10 stirred at 1400 rpm.

According to the SEM microgrphs, the microspheres produced with 600 rpm stirring speed exhibited a 100-1000 μm size range. Increasing the mixing speed from 600 rpm to 1000 rpm decreased the size range to 100-600 μm. The highest stirring speed 1400 rpm exhibited the size-reduced microspheres and more uniform size range between the range of 100 to 400 μm.

A new set of microspheres were prepared based on stirring speed experiment. The emulsion temperature was this time increased to 37 °C from room temperature, and the mixing speed was kept constant as 1400 rpm. The viscosity of the continuous phase (oil) was reduced when the temperature was increased. The measured oil viscosity values as function of temperature are shown in Table 4.1.

Table 4.1: Viscosity of the oil phase with respect to temperature.

| **Temperature (°C)** | **Viscosity (cP)** |
|---|---|
| 25 | 40.30 |
| 37 | 24.65 |

Decreased viscosity resulted a change in shear forces in the system during stirring. Therefore, increasing the temperature from 25 °C to 37 °C caused a viscosity change, and a dramatic size reduction that could not be obtained by adjusting the stirring rate. The microspheres prepared at higher temperature (37 °C) and stirring speed exhibited the smallest microspheres and the best uniform size distribution.The SEM micrographs indicating the morphology of the microspheres are two different oil temperature are shown in Figure 4.14. According to the SEM micrographs in Figure 4.14, the microspheres with a diameter of 100-400 μm that were produced at 25 °C, exhibited a size reduction to 20-200 μm and the most uniform size distrubution.

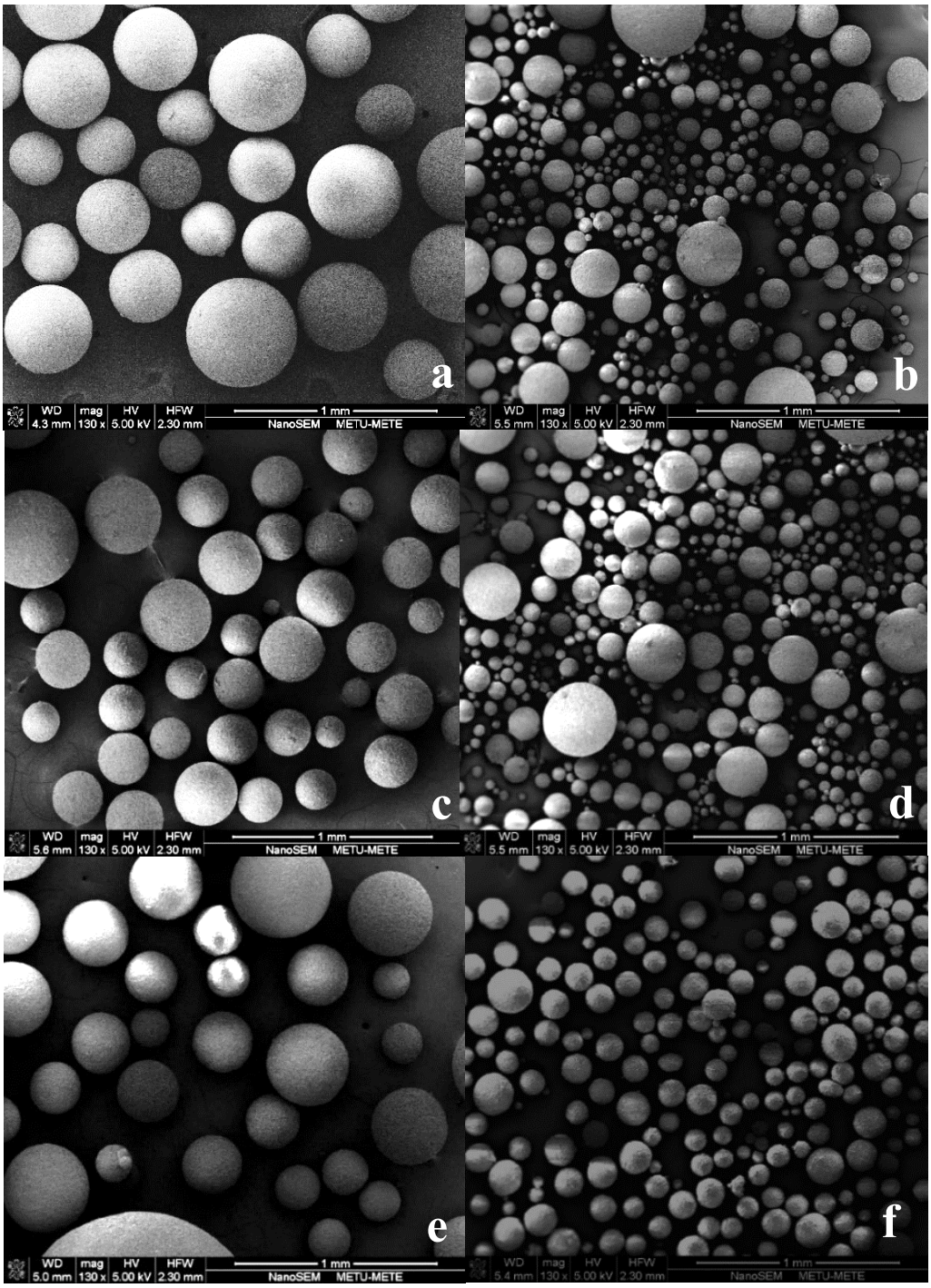



Figure 4.14: SEM micrographs of a)TCP/G-5 at 25 °C, b) TCP/G-5 at 37 °C, c) TCP/G-7.5 at 25 °C, d) TCP/G-7.5 at 37 °C, e) TCP/G-10 at 25 °C, and f)TCP/G-10 at 37 °C.

#### 4.2.2.2 Effect of Composition and Hydration Media on Cement Conversation (gelatin amount, water vs phosphate buffer solution - PBS

The preformed TCP/Gelatin microspheres with different gelatin content were hydrated for 2 h, 6 h, 12 h, 24 h, and 48 h both in DI water and phosphate buffer solution (PBS) at 37 °C to induce the hydration based cement reaction in order to convert α-TCP to CDHAp. The hydration reaction of α-TCP→CDHAp was monitored with XRD to examine the phase characteristics at different hydration time intervals (2 h to 48 h). The XRD data showed that the TCP/Gelatin microspheres with all gelatin compositions were hydrated at the end of 24 h as can be seen from the diffratograms in Figure 4.15. The 24 h XRD patterns reveal phase pure hydration product-CDHAp, whereas 12 h patterns indicate a binary phase mixture of unreacted TCP and partially hydrated CDHAp. The hydration of α-TCP to CDHAp seems to be completed at some point between 12 h and 24 h. The XRD diffractograms of the complete data set (2 h to 48 h), i.e. as a function of hydration time for each microsphere composition are provided in *Appendix A and Appendix B.*

The SEM micrograph, as a representative information, in Figure 4.16 show the microstructural detail of the surface for 24 h hydrated TCP/G-5. The cement products' appearance is quite different than initial morphology of α-TCP particles. Similar to XRD-based findings, revealing a complete transformation to CDHAp, formation of reticulated plate-like, flake crystals is indicative for formation of CDHAp after complete hydration α-TCP. In fact, this characteristic morphological change yields to cement-type hardening.

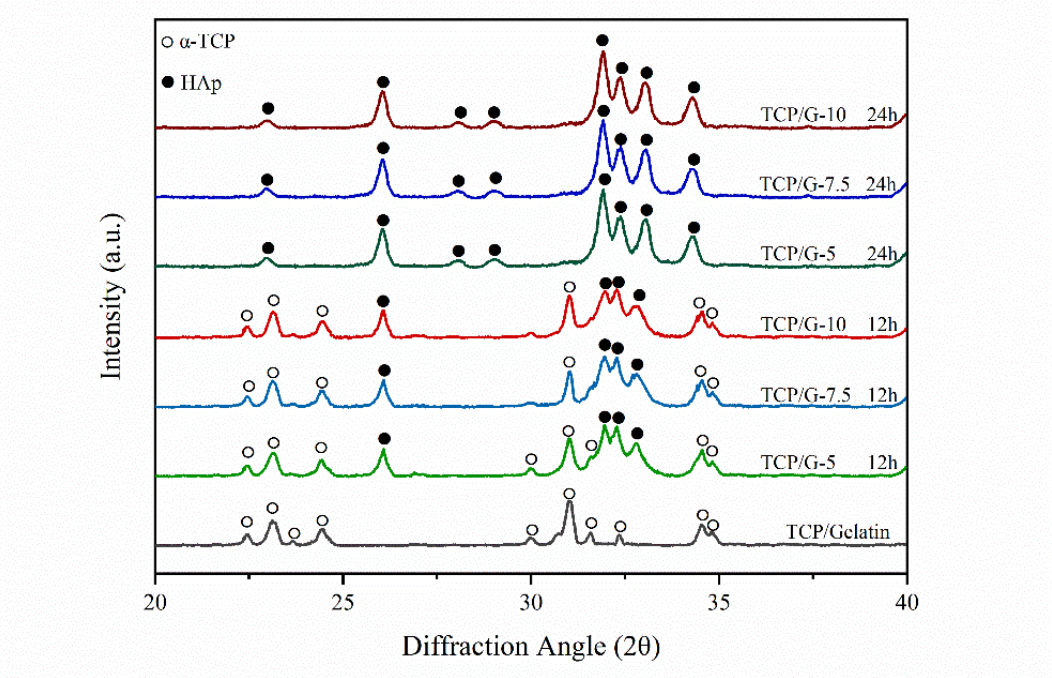



Figure 4.15: The XRD diffractograms of 12 h and 24 h hydrated TCP/G-5, TCP/G-7.5, and TCP/G-10.

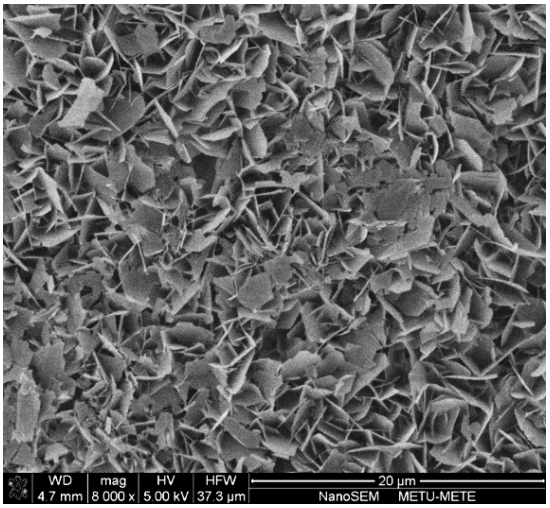



Figure 4.16. SEM micrograph of 24 h hydrated TCP/G-5 microsphere.

In regard to studies with the alternative hydration media using PBS, it was found that the microspheres were converted to CDHAp faster than the ones that were hydrated in DI water. The conversion to CDHAp occurred faster in the ionic media than DI water due to the common ion effect (presence of the ionic group relavat to HAp. Such as $PO_4^{3-}$) The common ion, phosphate ions in the buffer solution in this case, leads to a higher initial saturation degree, normally requires ion release by dissolution of TCP. Pre-existing ions provide faster kinetic for the dissolution and reprecipitation controlled cement hydration. The XRD diffractograms of TCP/Gelatin microspheres 6 h hydration in the PBS are shown in Figure 4.17. According to the XRD diffractograms, TCP/G-5 composition was the only one that was fully converted to HAp in 6 h when PBS was used as the aqueous media. This was more than 12 h in case hydration with DI-water. TCP/G-7.5 and TCP/G-10 microspheres however still contain some unreacted α-TCP; but in lower amount compared to DI-water hydrated counterparts. The complete XRD data of each composition hydrated in PBS as a function of time is provided in *Appendix B.* The other compositions (TCP/G-7.5 and TCP/G-10) completed the hydration reaction in 12 h. Based on the results, a higher binder amount, here higher gelatin content effects the hydration efficiency negatively.

The microspheres were analyzed with FTIR to detect any change in the structure of the organic component gelatin during the hydration. The FTIR spectra of the TCP/Gelatin microspheres after hydration in DI water for 48 h are shown in Figure 4.18. The chemical composition change possibility of the gelatin was elucidated based on the FTIR data. The bands of gelatin remained at the same position (1590 $cm^{-1}$ and 1630 $cm^{-1}$). According to the data, cross-linked gelatin remained undissolved/unchanged in the aqueous environment. In all hydration products, regardless of gelatin amount, characteristics band at 880 $cm^{-1}$ of the hydrated inorganic constituent proves that the HAp formed upon hydration was not the stoichiometric HAp, but calcium-deficient HAp. (CDHAp, $Ca_9(HPO_4)(PO_4)_5(OH)$).

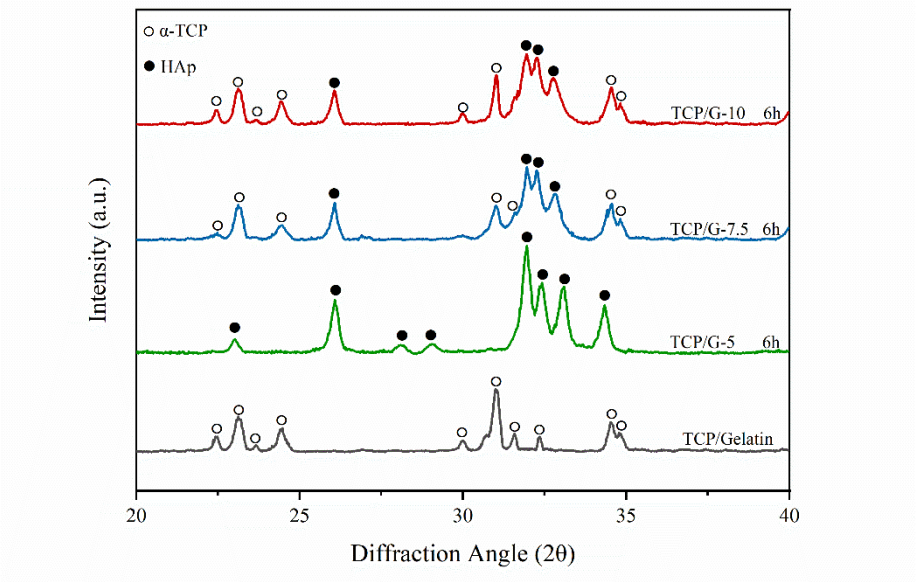



Figure 4.17: XRD diffractograms of 6 h hydrated TCP/G-5, TCP/G-7.5, TCP/G-10 in phosphate buffer solution.

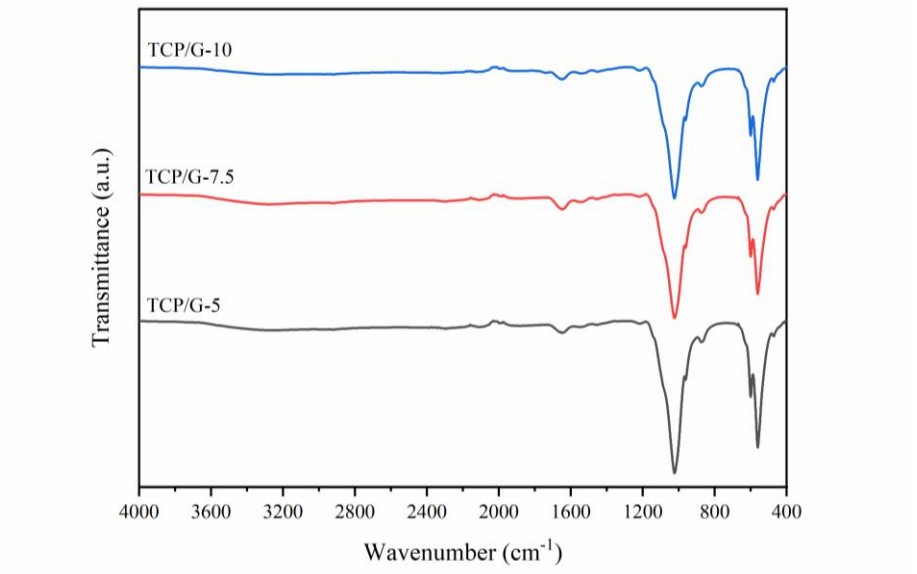



Figure 4.18: FTIR spectra of hydrated TCP/G-5, TCP/G-7.5, and TCP/G-10.

#### 4.2.2.3 Mechanical Properties of TCP/Gelatin Composites

A diametral compression test was applied to dummy coin shaped TCP/Gelatin pellets with identical processing history of the microsphers formed to evaluate the mechanical properties of the microspheres with different gelatin concentrations. Initially, non-hydrated samples were subjected to diametral compression.

The test results in Figure 4.19, indicate that increased gelatin concentration slightly increased the diametral compressive strength. As rough range the strength varies 2.7-4.50 MPa depending on the gelatin content for non-hydrated condition.

The results in Figure 4.20, on the other hand exhibit the 48 h hydrated samples' diametral compression strength that were hydrated in DI water. This time the strength values roughly doubles for each composition and approximately ranges form 4.9-10.30 MPa. The strength gain is an expected and natural consequence of cement conversion (effective hydration). In Table 4.3, diametral compressive strength of each composition are provided. Natural bone properties are shown in Table 4.2 for comparison.

According to the literatura data, the diametral tensile strength of the TCP/Gelatin pellets are in the tensile strength range of natural bone. Depending on the highest gelatin concentration, TCP/G-10 pellets reach the upper bound of cancellous bone's tensile strength. After hydration, TCP/Gelatin samples all reach the upper bound oF the tensile strength of cancellous bone. TCP/G-7.5 and TCP/G-10 compositions exceed the literature value.

Table 4.2: Natural bone properties.

| Type of Bone | Compressive Strength (MPa) | Tensile Strength (MPa) |
|---|---|---|
| Cortical Bone | 100-230 [68] | 50-150 [69, 70] |
| Cancellous Bone | 2-12 [68] | 1-5 [70] |

Table 4.3: Diametral tensile strength of TCP/G-5, TCP/G-7.5 and TCP/G-10.

| Composition | Diametral Tensile Strength (non-hydrated) (MPa) | Diametral Tensile Strength (hydrated) (MPa) |
|---|---|---|
| **TCP/G-5** | 2.7 ±0.4 | 4.9±0.4 |
| **TCP/G-7.5** | 4.1±0.4 | 8.0 ±0.9 |
| **TCP/G-10** | 4.5±0.9 | 10.3±0.3 |

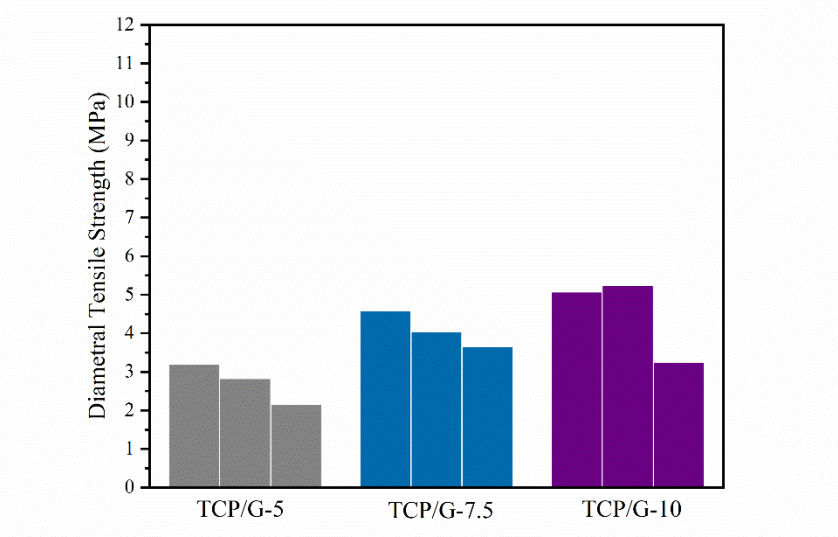



Figure 4.19: Diametral tensile strength data of non-hydrated TCP/G-5, TCP/G-7.5, and TCP/G-10.

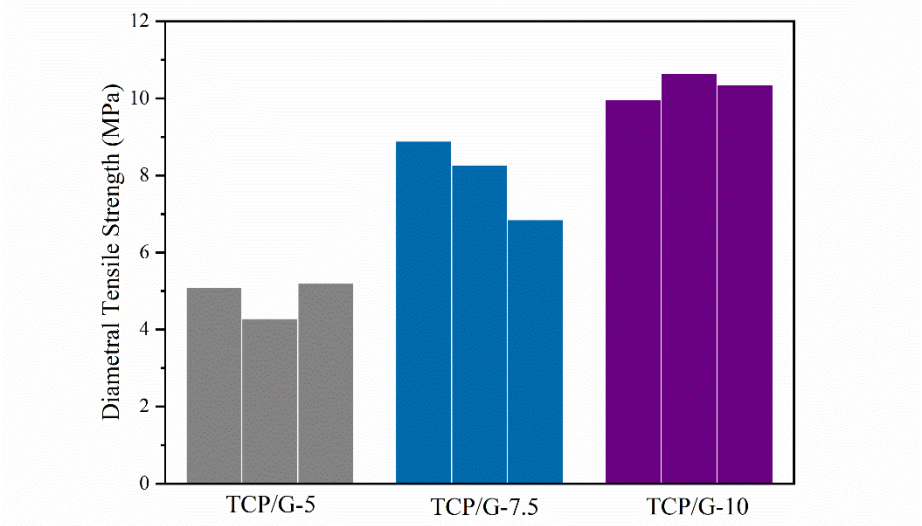



Figure 4.20: Diametral tensile strength data of hydrated TCP/G-5, TCP/G-7.5, and TCP/G-10.

## 4.3 Characterization of TCP/CSH (TCP:Calcium Sulfate Hemihydrate) Hybrid Microspheres

A hybrid cement formulation using another cement together with TCP, i.e. calcium-sulfate, has been also formed. The intention was to improve strength of the microspheres further by combining two parallel hydration events, both leading cement-type hardening. Calcium sulfate hemihydrate also exhibit an intrinsic cement-type conversion similar to α-TCP. These microspheres were produced with two different compositions. The compositional effects on the hydration were examined by reaction time-based XRD and SEM analyses. Two compositions, CS10 (90 wt.% TCP:10 wt.% CSH) and CS25 (75 wt.% TCP:25 wt.% CSH) were investigated and compared in terms of sphere formation behavior, microstructure and mechanical properties.

The hydration time-dependent XRD diffractograms of CS10 and CS25 microspheres are provided in Figure 4.21 and Figure 4.22, respectively. Both compositions were hydrated in DI water and PBS. The XRD data indicate a suppressed hydration efficiency for TCP for both compositions and α-TCP was not completely converted to CDHAp after 48 h. This effect was more pronounced in the case DI-water hydrated samples.

According to the XRD data, both CS10 and CS25's calcium sulfate hemihydrate (CSH) phase was fully converted to calcium sulfate dihydrate (CSD) even during the preparation of microspheres in the emulsion system (as-prepared). The slurry preparation and cross-linking were both aqueous routes, therefore CSH set as CSD during those processes. Typically setting of CSH compared to TCP occurs much faster.

After 48 h of hydration in $H_2O$, both CS10 and CS25 were only partially converted to CDHAp. The hydration products in $H_2O$ exhibited different phases depending on the calcium sulfate amount. The calcium sulfate phase of CS10 was completely dissolved in $H_2O$. However, calcium sulfate dihydrate and calcium sulfate anhydrous

phases were still present in 48 h hydrated CS25. The CS10, and CS25 exhibited the similar behavior when hydrated in PBS. In that case, both CS10 and CS25 were fully converted to CDHAp, and calcium sulfate anhydrous phase was only present in CS25. The results indicate that calcium sulfate phase remained in the CS10 completely dissolved after complete hydration, and CDHAp was the only phase remained. The calcium sulfate phase in the CS25 did not fully dissolve even after the additional hydration process. The amount of the calcium phosphate has an influence on the final product.

The morphology of the final products was analyzed with SEM. The SEM micrographs indicating the surface morphology of the hydration products of CS10 and CS25 are provided in Figure 4.23 and Figure 4.24, respectively. The mentioned SEM micrographs exhibit surface pores formed upon dissolution of calcium sulfate phase. This microstructural features were not observed for the microspheres formed by sole use of TCP.

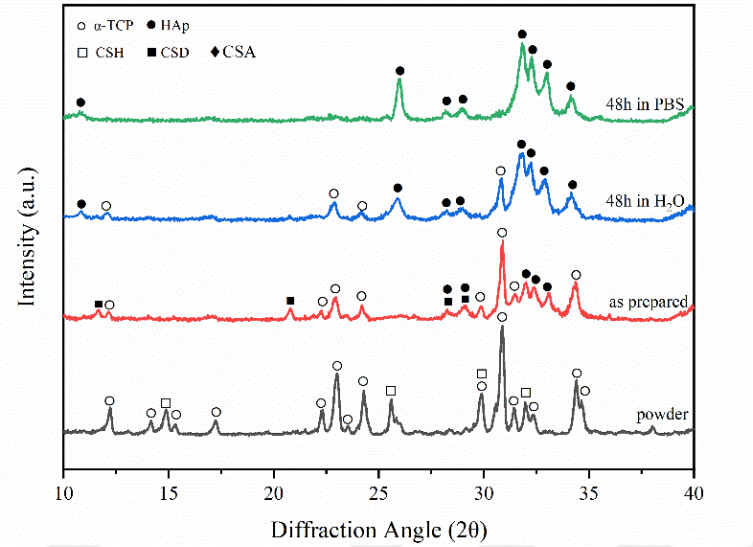



Figure 4.21: XRD diffractograms of CS25 powder, as-prepared CS25 microspheres as-prepared, hydrated CS25 microspheres for 48h in $H_2O$, and hydrated CS25 microspheres for 48 h in PBS.

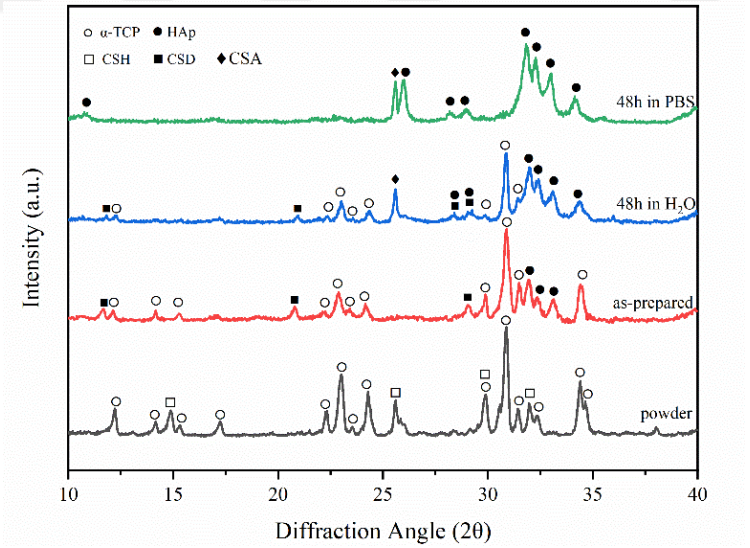



Figure 4.22: XRD diffractograms of CS25 powder, as-prepared CS25 microspheres as-prepared, hydrated CS25 microspheres for 48 h in $H_2O$, and hydrated CS25 microspheres for 48 h in PBS.

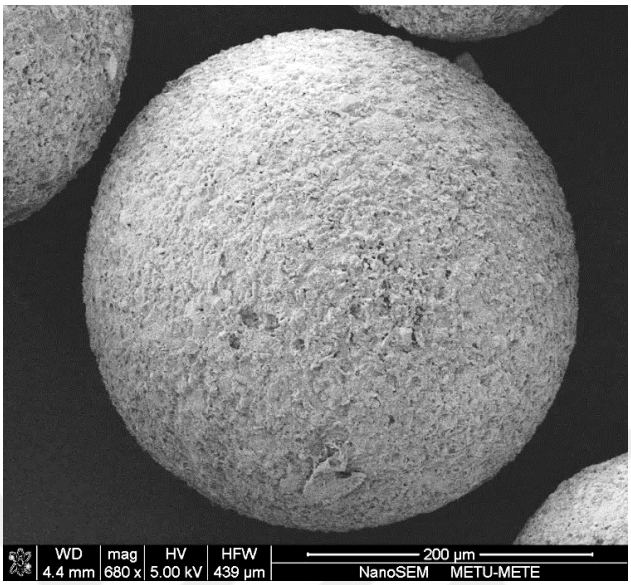



Figure 4.23: SEM micrograph of hydrated CS10.

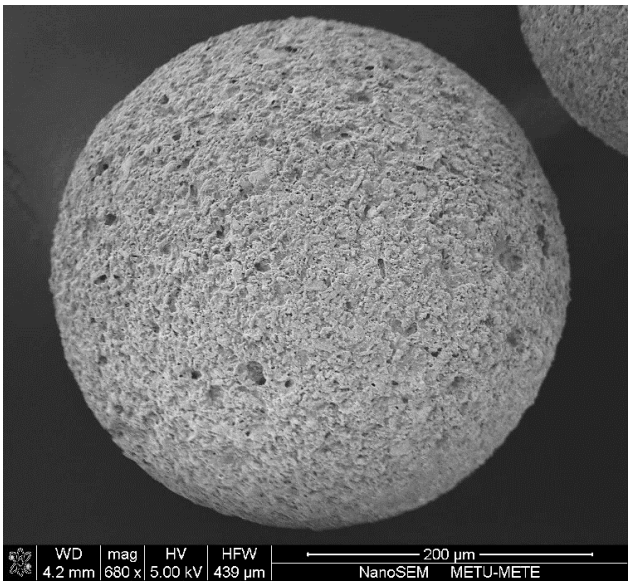



Figure 4.24: SEM micrograph of hydrated CS25.

The chemical structure of the CS10 and CS25 microspheres were investigated with FTIR analyses. The non-hydrated powders, and the hydration products were examined. The FTIR spectra of showing hydration products of CS10 and CS25 are shown in Figure 4.25. According to the FTIR spectra, organic gelatin phase was remained after hydration in both $H_2O$, and PBS. The Amide I, and Amide II bands are visible. According to the CS10's FTIR spectra, the calcium sulfate phase band visible at 610 $cm^{-1}$ wavenumber was disappeared after hydration. The same band of CS25 remained after hydration in both $H_2O$ and PBS. These results correlate with the XRD data, with an additional knowledge of gelatin presence after hydration.

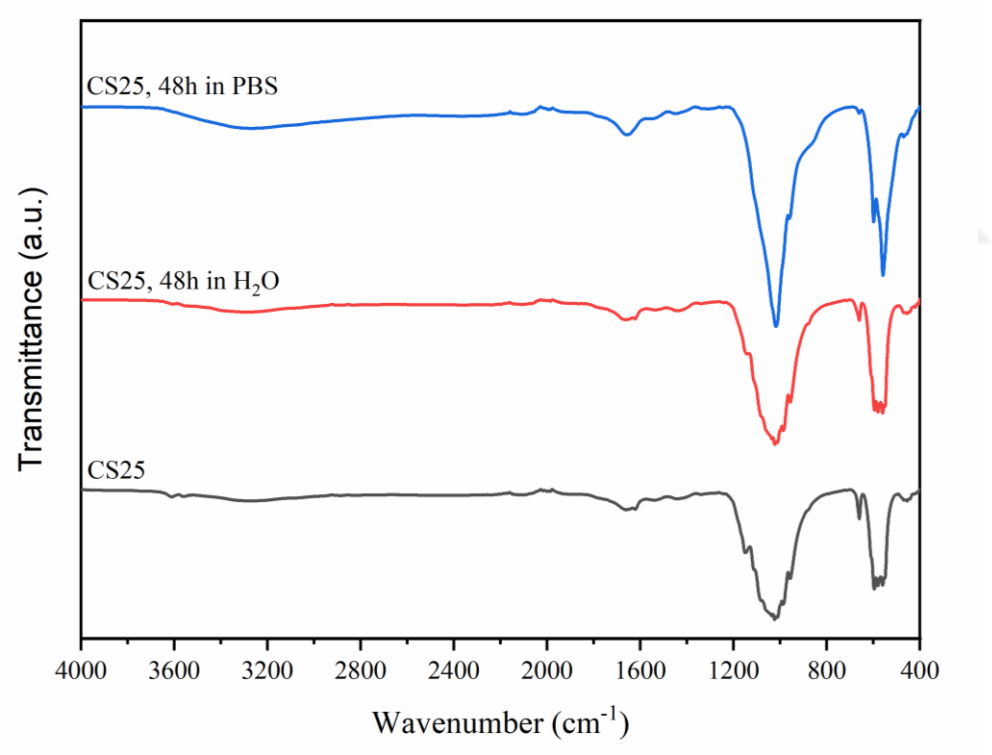



Figure 4.25: FTIR spectra of CS25, and its hydration products in different aqueous media ($H_2O$ and PBS).

### 4.3.1 Mechanical Properties of TCP/CS Microspheres

The mechanical properties of the hydration products of CS10 and CS25 were evaluated and compared with the hydration product of TCP/G-5. The TCP/G-5 that was hydrated in DI water for 48 h was taken as a basis due to its same amount of gelatin content as CS10 and CS25. The CS10 and CS25 test samples were hydrated in PBS for 48 h for complete hydration.

The diametral test results in Figure 4.26 indicate that the hydration products of TCP/CS hybrids exhibit poor mechanical characteristics and strength when compared with only TCP-containing counterparts. The strength of only TCP containing microsphere was around 5 MPa. The dual cement containing microspheres reach only 3.5 MPa. The diametral compressive strength of hydration products of TCP/CS, exhibit a slight decrease with increasing calcium sulfate concentration.

These findings show that the porosity created by the dissolution of calcium sulfate component invalidate the initial postulation in regard to using a dual cement for strength improvement. However, such approach can be used and can be adapted in developing porous microspheres with controlled porosity. This can be useful in improving the functional properties of a bioceramic-based microsphere due to a better integration bone cells and bone tissue. In Table 4.4, the diametral compressive strength of each sample are provided. According to the natural bone properties that shown in Table 4.2, the diametral tensile strength values of CS10 and CS25 are both in the tensile strength range of the cancellous bone.

Table 4.4: Diametral tensile strength of hydrated TCP/G-5, CS10 and CS25.

| Composition | Diametral Tensile Strength (MPa) |
|---|---|
| TCP/G-5 | 4.9±0.4 |
| CS10 | 3.7±0.1 |
| CS25 | 3.4±1.1 |

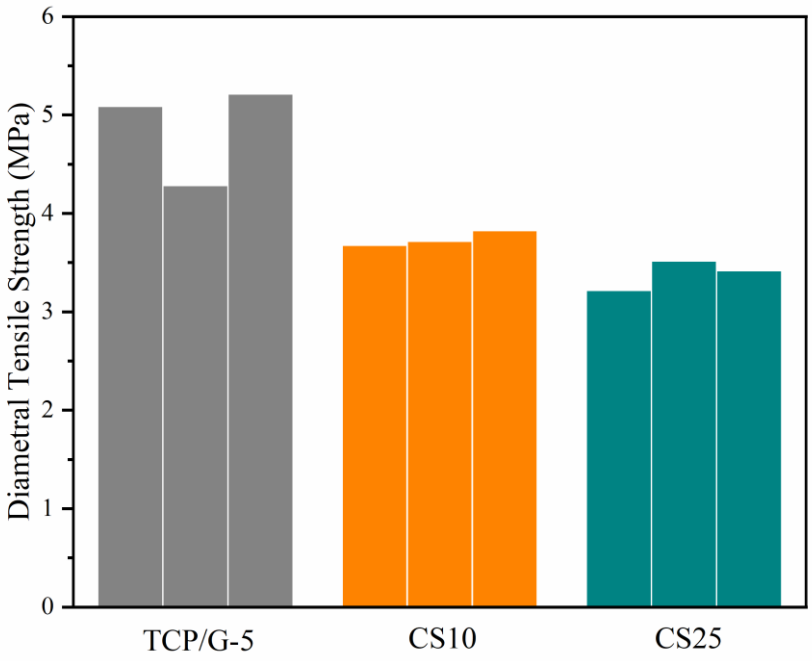



Figure 4.26: Diametral tensile strength of hydrated TCP/G-5, CS10, and CS25.

# CHAPTER 5

# CONCLUSIONS

Phase pure α-TCP was synthesized by solid-state reaction of chemically synthesized monetite ($CaHPO_4$) and calcium carbonate ($CaCO_3$) at 1200 °C for 2 h. The composite microspheres were formed by incorporation of organic alginate and gelatin polymers/binders to α-TCP. The effect of the binders on morphology, size, and cement-type reactivity were examined. The α-TCP and calcium sulfate hemihydrate (CSH, $CaSO_4 \cdot {}^1/_2H_2O$) hybrid microspheres were developed with different compositions, and the compositional effect on cement-type reactivity was examined.

## α-TCP/Polymer Composite Microspheres

α-TCP/Polymer composite microspheres were developed with Na-Alginate:Water (2 wt.%) and Gelatin:Water (5 wt.%, 7.5 wt.%, and 10 wt.%) solutions by emulsion-based processing. $\alpha$-TCP/Alginate microspheres exhibited structural defects, shape distortion, and agglomeration. Alginate found to be not a proper binding agent. Gelatin, a binding agent, was sufficient to form the well-defined spherical shape regardless of the concentration. The emulsion parameters were adjusted to obtain microspheres with reduced size. The highest stirring rate 1400 rpm was found to be the appropriate option to obtain the smallest microspheres. The temperature change from 25 °C to 37 °C decreased the viscosity from 40.30 cP to 24.65 cP, and dramatic size reduction was observed. The hydration profile of $\alpha$-TCP/Gelatin microspheres with different gelatin concentrations (5 wt.%, 7.5 wt.%, and 10 wt.%) were examined in DI water and PBS. Each concentration exhibited a complete CDHAp (calcium-deficient HAp) conversion in 24 h in DI water. The $\alpha$-TCP to CDHAp conversion time was reduced to 12 h in PBS. The microspheres formed with 5 wt.% gelatin

solution was the only composition that was converted to CDHAp in 6 h in PBS. The conversion rate was decreased with the decreasing gelatin concentration. The diametral compressive strenght of the microspheres exhibited an improvement with the increased gelatin concentration and hydration.

**α-TCP/CSH Hybrid Microspheres**

α-TCP/CSH composite microspheres were developed in two different composition

. The two compositions, CS10 (90 wt.% TCP:10 wt.% CSH) and CS25 (75 wt.% TCP:25 wt.% CSH) were both insufficient to convert to CDHAp in DI water in 48 h. Both of the composition exhibited a complete conversion to CDHAp only in PBS in 48 h. The calcium sulfate phase of both compositions were partially or completely dissolved in the aqueous environment during the hydration, and created a porous morphology. The CS25 was the only composition that calcium sulfate phase was remained after hydration in both aqueous media. The highest initial calcium sulfate concentration resulted a decreased diametral compressive strength of the hydration product.

## REFERENCES


[1] M. J. Olszta *et al.*, "Bone structure and formation: A new perspective," *Mater. Sci. Eng. R Rep.*, vol. 58, no. 3–5, pp. 77–116, 2007.

[2] B. Clarke, "Normal bone anatomy and physiology," *Clin. J. Am. Soc. Nephrol.*, vol. 3 Suppl 3, no. Supplement 3, pp. S131-9, 2008.

[3] R. Murugan and S. Ramakrishna, "Development of nanocomposites for bone grafting," *Compos. Sci. Technol.*, vol. 65, no. 15–16, pp. 2385–2406, 2005.

[4] N. Reznikov, R. Shahar, and S. Weiner, "Bone hierarchical structure in three dimensions," *Acta Biomater.*, vol. 10, no. 9, pp. 3815–3826, 2014.

[5] S. Weiner and H. D. Wagner, "THE MATERIAL BONE: Structure-mechanical function relations," *Annu. Rev. Mater. Sci.*, vol. 28, no. 1, pp. 271–298, 1998.

[6] J. Y. Rho, L. Kuhn-Spearing, and P. Zioupos, "Mechanical properties and the hierarchical structure of bone," *Med. Eng. Phys.*, vol. 20, no. 2, pp. 92–102, 1998.

[7] S. V. Dorozhkin, "Biocomposites and hybrid biomaterials based on calcium orthophosphates," *Biomatter*, vol. 1, no. 1, pp. 3–56, 2011.

[8] C. Burger *et al.*, "Lateral packing of mineral crystals in bone collagen fibrils," *Biophys. J.*, vol. 95, no. 4, pp. 1985–1992, 2008.

[9] E. E. Wilson, A. Awonusi, M. D. Morris, D. H. Kohn, M. M. J. Tecklenburg, and L. W. Beck, "Three structural roles for water in bone observed by solid-state NMR," *Biophys. J.*, vol. 90, no. 10, pp. 3722–3731, 2006.

[10] P. Fratzl and R. Weinkamer, “Nature’s hierarchical materials,” *Prog. Mater. Sci.*, vol. 52, no. 8, pp. 1263–1334, 2007.

[11] “Calcium Orthophosphates as Bioceramics,” in *Calcium Orthophosphates*, Pan Stanford Publishing, 2012, pp. 329–458.

[12] T. Albrektsson and C. Johansson, “Osteoinduction, osteoconduction and osseointegration,” in *The Use of Bone Substitutes in Spine Surgery*, Berlin, Heidelberg: Springer Berlin Heidelberg, 2002, pp. 12–17.

[13] P. Baldwin, D. J. Li, D. A. Auston, H. S. Mir, R. S. Yoon, and K. J. Koval, “Autograft, allograft, and bone graft substitutes: Clinical evidence and indications for use in the setting of orthopaedic trauma surgery: Clinical evidence and indications for use in the setting of orthopaedic trauma surgery,” *J. Orthop. Trauma*, vol. 33, no. 4, pp. 203–213, 2019.

[14] V. Campana *et al.*, “Bone substitutes in orthopaedic surgery: from basic science to clinical practice,” *J. Mater. Sci. Mater. Med.*, vol. 25, no. 10, pp. 2445–2461, 2014.

[15] N. Saulacic, M. Fujioka-Kobayashi, Y. Kimura, A. I. Bracher, C. Zihlmann, and N. P. Lang, “The effect of synthetic bone graft substitutes on bone formation in rabbit calvarial defects,” *J. Mater. Sci. Mater. Med.*, vol. 32, no. 1, p. 14, 2021.

[16] D. Offner *et al.*, “Bone grafts, bone substitutes and regenerative medicine acceptance for the management of bone defects among French population: Issues about ethics, religion or fear?,” *Cell Med.*, vol. 11, p. 2155179019857661, 2019.

[17] H. H. K. Xu *et al.*, “Calcium phosphate cements for bone engineering and their biological properties,” *Bone Res.*, vol. 5, no. 1, p. 17056, 2017.

[18] T. T. Roberts and A. J. Rosenbaum, “Bone grafts, bone substitutes and orthobiologics: the bridge between basic science and clinical advancements in fracture healing: The bridge between basic science and clinical

advancements in fracture healing," *Organogenesis*, vol. 8, no. 4, pp. 114–124, 2012.

[19] H.-S. Sohn and J.-K. Oh, "Review of bone graft and bone substitutes with an emphasis on fracture surgeries," *Biomater. Res.*, vol. 23, no. 1, p. 9, 2019.

[20] Y.-H. Chiu, I.-C. Chen, C.-Y. Su, H.-H. Tsai, T.-H. Young, and H.-W. Fang, "Development of injectable calcium sulfate and self-setting calcium phosphate composite bone graft materials for minimally invasive surgery," *Int. J. Mol. Sci.*, vol. 23, no. 14, p. 7590, 2022.

[21] W. R. Moore, S. E. Graves, and G. I. Bain, "Synthetic bone graft substitutes: Synthetic Bone Graft Substitutes," *ANZ J. Surg.*, vol. 71, no. 6, pp. 354–361, 2001.

[22] S. K. Nandi, S. Roy, P. Mukherjee, B. Kundu, D. K. De, and D. Basu, "Orthopaedic applications of bone graft & graft substitutes: a review," *Indian J. Med. Res.*, vol. 132, pp. 15–30, 2010.

[23] S. V. Dorozhkin, "Bioceramics of calcium orthophosphates," *Biomaterials*, vol. 31, no. 7, pp. 1465–1485, 2010.

[24] S. V. Dorozhkin, "Calcium orthophosphates as bioceramics: state of the art," *J. Funct. Biomater.*, vol. 1, no. 1, pp. 22–107, 2010.

[25] K. Ishikawa, "Calcium Phosphate Cement," in *Springer Series in Biomaterials Science and Engineering*, Berlin, Heidelberg: Springer Berlin Heidelberg, pp. 199–227, 2014.

[26] S. Dorozhkin, "Calcium orthophosphates in nature, biology and medicine," *Materials (Basel)*, vol. 2, no. 2, pp. 399–498, 2009.

[27] G. Fernandez de Grado *et al.*, "Bone substitutes: a review of their characteristics, clinical use, and perspectives for large bone defects management," *J. Tissue Eng.*, vol. 9, p. 2041731418776819, 2018.

[28] T. V. Safronova *et al.*, "Biocompatibility of biphasic α,β-tricalcium phosphate ceramics in vitro," *Bioact. Mater.*, vol. 5, no. 2, pp. 423–427, 2020.

[29] R. G. Carrodeguas and S. De Aza, "α-Tricalcium phosphate: synthesis, properties and biomedical applications," *Acta Biomater.*, vol. 7, no. 10, pp. 3536–3546, 2011.

[30] C. L. Camire', S. Jegou Saint-Jean, S. Hansen, I. McCarthy, and L. Lidgren, "Hydration characteristics of alpha-tricalcium phosphates: Comparison of preparation routes," *J. Appl. Biomater. Biomech.*, vol. 3, no. 2, pp. 106–111, 2005.

[31] A.-M. Yousefi, "A review of calcium phosphate cements and acrylic bone cements as injectable materials for bone repair and implant fixation," *J. Appl. Biomater. Funct. Mater.*, vol. 17, no. 4, p. 2280800019872594, 2019.

[32] G. Lewis, "Injectable bone cements for use in vertebroplasty and kyphoplasty: state-of-the-art review," *J. Biomed. Mater. Res. B Appl. Biomater.*, vol. 76, no. 2, pp. 456–468, 2006.

[33] K. Ishikawa, "Bone substitute fabrication based on dissolution-precipitation reactions," *Materials (Basel)*, vol. 3, no. 2, pp. 1138–1155, 2010.

[34] D. Apelt *et al.*, "In vivo behavior of three different injectable hydraulic calcium phosphate cements," *Biomaterials*, vol. 25, no. 7–8, pp. 1439–1451, 2004.

[35] J. Zhang, W. Liu, V. Schnitzler, F. Tancret, and J.-M. Bouler, "Calcium phosphate cements for bone substitution: chemistry, handling and mechanical properties," *Acta Biomater.*, vol. 10, no. 3, pp. 1035–1049, 2014.

[36] S. Dorozhkin, "Calcium orthophosphate cements and concretes," *Materials (Basel)*, vol. 2, no. 1, pp. 221–291, 2009.

[37] M. Bohner, T. J. Brunner, and W. J. Stark, “Controlling the reactivity of calcium phosphate cements,” *Key Eng. Mater.*, vol. 361–363, pp. 295–298, 2007.

[38] M. Stevanović, J. Savić, B. Jordović, and D. Uskoković, “Fabrication, in vitro degradation and the release behaviours of poly(DL-lactide-co-glycolide) nanospheres containing ascorbic acid,” *Colloids Surf. B Biointerfaces*, vol. 59, no. 2, pp. 215–223, 2007.

[39] M. Nilsson, E. Fernández, S. Sarda, L. Lidgren, and J. A. Planell, “Characterization of a novel calcium phosphate/sulphate bone cement: Novel Calcium Phosphate/Sulphate Bone Cement,” *J. Biomed. Mater. Res.*, vol. 61, no. 4, pp. 600–607, 2002.

[40] M. Bohner, “New hydraulic cements based on α-tricalcium phosphate–calcium sulfate dihydrate mixtures,” *Biomaterials*, vol. 25, no. 4, pp. 741–749, 2004.

[41] O. Fraile-Martínez *et al.*, “Applications of polymeric composites in bone tissue engineering and jawbone regeneration,” *Polymers (Basel)*, vol. 13, no. 19, p. 3429, 2021.

[42] A. Ficai, E. Andronescu, G. Voicu, and D. Ficai, “Advances in Collagen/Hydroxyapatite Composite Materials,” in *Advances in Composite Materials for Medicine and Nanotechnology*, InTech, 2011.

[43] S. P. Victor and J. Muthu, “Polymer ceramic composite materials for orthopedic applications-relevance and need for mechanical match and bone regeneration,” *J. Mechatron.*, vol. 2, no. 1, pp. 1–10, 2014.

[44] J. Jeong, J. H. Kim, J. H. Shim, N. S. Hwang, and C. Y. Heo, “Bioactive calcium phosphate materials and applications in bone regeneration,” *Biomater. Res.*, vol. 23, no. 1, p. 4, 2019.

[45] K. T. Arul, E. Manikandan, and R. Ladchumananandasivam, “Polymer-based calcium phosphate scaffolds for tissue engineering applications,” in *Nanoarchitectonics in Biomedicine*, Elsevier, pp. 585–618, 2019.

[46] W. J. E. M. Habraken, L. T. de Jonge, J. G. C. Wolke, L. Yubao, A. G. Mikos, and J. A. Jansen, "Introduction of gelatin microspheres into an injectable calcium phosphate cement," *J. Biomed. Mater. Res. A*, vol. 87, no. 3, pp. 643–655, 2008.

[47] W. J. E. M. Habraken, J. G. C. Wolke, A. G. Mikos, and J. A. Jansen, "Porcine gelatin microsphere/calcium phosphate cement composites: an in vitro degradation study," *J. Biomed. Mater. Res. B Appl. Biomater.*, vol. 91, no. 2, pp. 555–561, 2009.

[48] F. E. Baştan, "Production and Characterization of Gelatin Functianalized Hydroxyapatite Composite Microspheres for Biomedical Applications," *Eskişehir Technical University Journal of Science and Technology A - Applied Sciences and Engineering*, 2021.

[49] A. Bigi, B. Bracci, and S. Panzavolta, "Effect of added gelatin on the properties of calcium phosphate cement," *Biomaterials*, vol. 25, no. 14, pp. 2893–2899, 2004.

[50] R. A. Perez, S. Del Valle, G. Altankov, and M.-P. Ginebra, "Porous hydroxyapatite and gelatin/hydroxyapatite microspheres obtained by calcium phosphate cement emulsion," *J. Biomed. Mater. Res. B Appl. Biomater.*, vol. 97, no. 1, pp. 156–166, 2011.

[51] S. Mofakhami and E. Salahinejad, "Biphasic calcium phosphate microspheres in biomedical applications," *J. Control. Release*, vol. 338, pp. 527–536, 2021.

[52] K. M. Z. Hossain, U. Patel, and I. Ahmed, "Development of microspheres for biomedical applications: a review," *Prog. Biomater.*, vol. 4, no. 1, pp. 1–19, 2015.

[53] M. Bohner, S. Tadier, N. van Garderen, A. de Gasparo, N. Döbelin, and G. Baroud, "Synthesis of spherical calcium phosphate particles for dental and orthopedic applications," *Biomatter*, vol. 3, no. 2, p. e25103, 2013.

[54] C. de O. Renó and M. Motisuke, “Optimizing the water-oil emulsification process for developing CPC microspheres,” *Mater. Res.*, vol. 19, no. 6, pp. 1388–1392, 2016.

[55] S. N. Kale and S. L. Deore, “Emulsion Micro Emulsion and Nano Emulsion: A Review,” *Syst. Rev. Pharm.*, vol. 8, no. 1, pp. 39–47, 2016.

[56] Y. Maphosa and V. A. Jideani, “Factors affecting the stability of emulsions stabilised by biopolymers,” in *Science and Technology Behind Nanoemulsions*, InTech, 2018.

[57] T. F. Tadros, “Emulsion Formation, Stability, and Rheology,” in *Emulsion Formation and Stability*, Weinheim, Germany: Wiley-VCH Verlag GmbH & Co. KGaA, 2013, pp. 1–75.

[58] G. Colucci, A. Santamaria-Echart, S. C. Silva, I. P. M. Fernandes, C. C. Sipoli, and M. F. Barreiro, “Development of water-in-oil emulsions as delivery vehicles and testing with a natural antimicrobial extract,” *Molecules*, vol. 25, no. 9, p. 2105, 2020.

[59] M. P. Ginebra, M. Espanol, E. B. Montufar, R. A. Perez, and G. Mestres, “New processing approaches in calcium phosphate cements and their applications in regenerative medicine,” *Acta Biomater.*, vol. 6, no. 8, pp. 2863–2873, 2010.

[60] E. Salimi and J. Javadpour, “Synthesis and characterization of nanoporous monetite which can be applicable for drug carrier,” *J. Nanomater.*, vol. 2012, pp. 1–5, 2012.

[61] B. Idowu, G. Cama, S. Deb, and L. Di Silvio, “In vitro osteoinductive potential of porous monetite for bone tissue engineering,” *J. Tissue Eng.*, vol. 5, p. 2041731414536572, 2014.

[62] A. Saarai, V. Kasparkova, T. Sedlacek, and P. Saha, “On the development and characterisation of crosslinked sodium alginate/gelatine hydrogels,” *J. Mech. Behav. Biomed. Mater.*, vol. 18, pp. 152–166, 2013.

[63] M. Fertah, A. Belfkira, E. M. Dahmane, M. Taourirte, and F. Brouillette, "Extraction and characterization of sodium alginate from Moroccan Laminaria digitata brown seaweed," *Arab. J. Chem.*, vol. 10, pp. S3707–S3714, 2017.

[64] H. Daemi and M. Barikani, "Synthesis and characterization of calcium alginate nanoparticles, sodium homopolymannuronate salt and its calcium nanoparticles," *Sci. iran.*, vol. 19, no. 6, pp. 2023–2028, 2012.

[65] M. A. El-Meligy, K. Valachová, I. Juránek, T. M. Tamer, and L. Šoltés, "Preparation and physicochemical characterization of gelatin-aldehyde derivatives," *Molecules*, vol. 27, no. 20, 2022.

[66] J. Lin, D. Pan, Y. Sun, C. Ou, Y. Wang, and J. Cao, "The modification of gelatin films: Based on various cross-linking mechanism of glutaraldehyde at acidic and alkaline conditions," *Food Sci. Nutr.*, vol. 7, no. 12, pp. 4140–4146, 2019.

[67] T.-H. Nguyen and B.-T. Lee, "Fabrication and characterization of cross-linked gelatin electro-spun nano-fibers," *J. Biomed. Sci. Eng.*, vol. 03, no. 12, pp. 1117–1124, 2010.

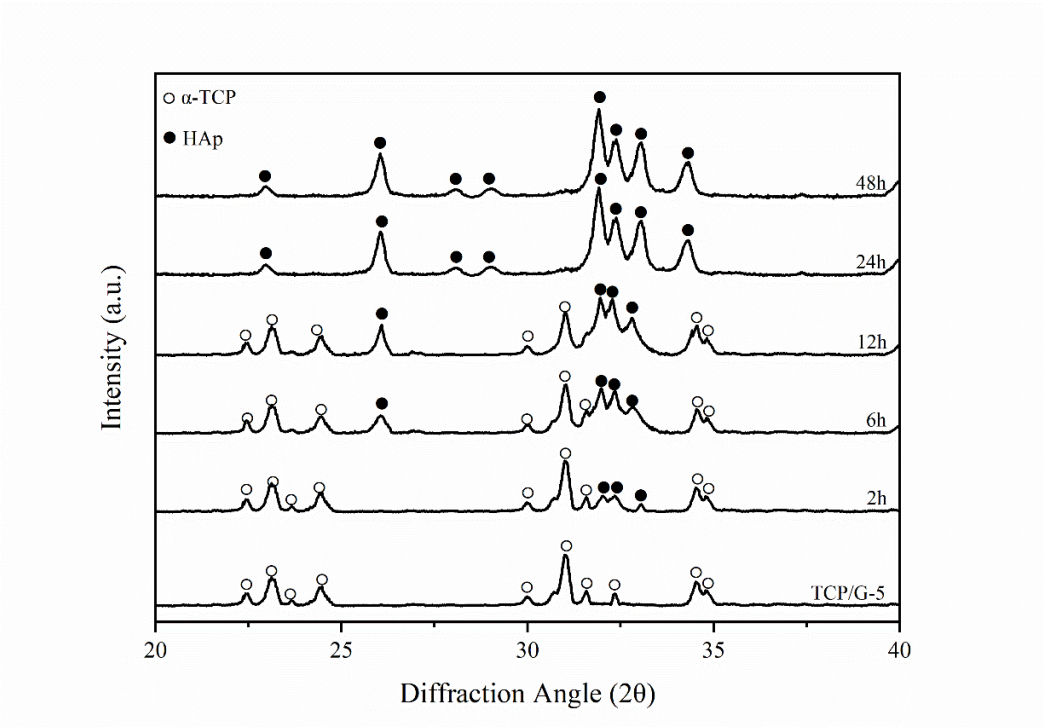
[68] N. A. Nawawi, A. S.F. Alqap, and I. Sopyan, "Recent progress on hydroxyapatite-based dense biomaterials for load bearing bone substitutes," *Recent pat. mater. sci.*, vol. 4, no. 1, pp. 63–80, 2011.

[69] J. Currey, "The structure and mechanical properties of bone," in Bioceramics and Their Clinical Applications, CRC Press, 2008.

[70] Q. Fu, E. Saiz, M. N. Rahaman, and A. P. Tomsia, "Toward strong and tough glass and ceramic scaffolds for bone repair," Adv. Funct. Mater., vol. 23, no. 44, pp. 5461–5476, 2013.

# APPENDICES

## A. TCP/Gelatin Hydration in DI Water




a

Figure A.1: The XRD diffractograms as a function of reaction time for TCP/G-5 in DI water.

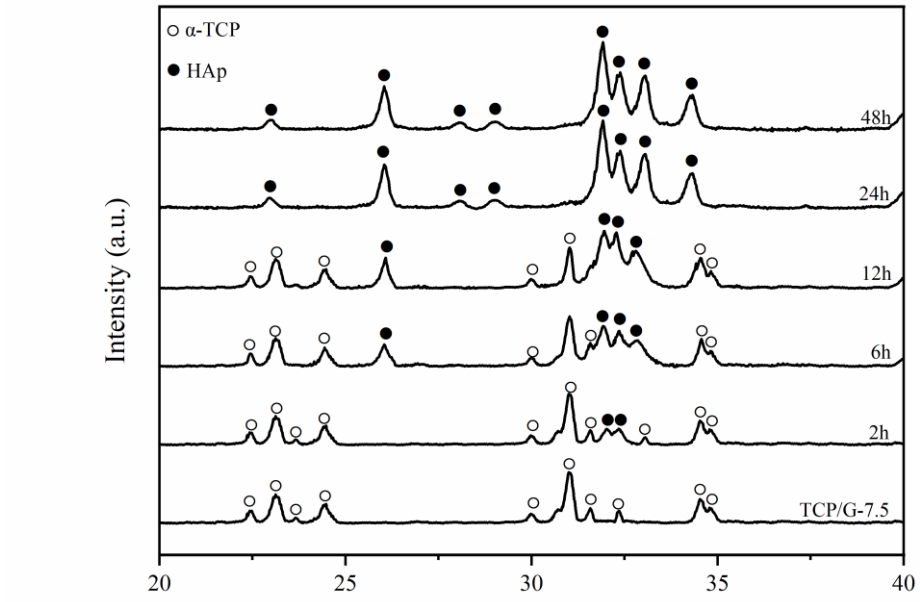



Figure A.2: The XRD diffractograms as a function of reaction time for TCP/G-7.5 in DI water.

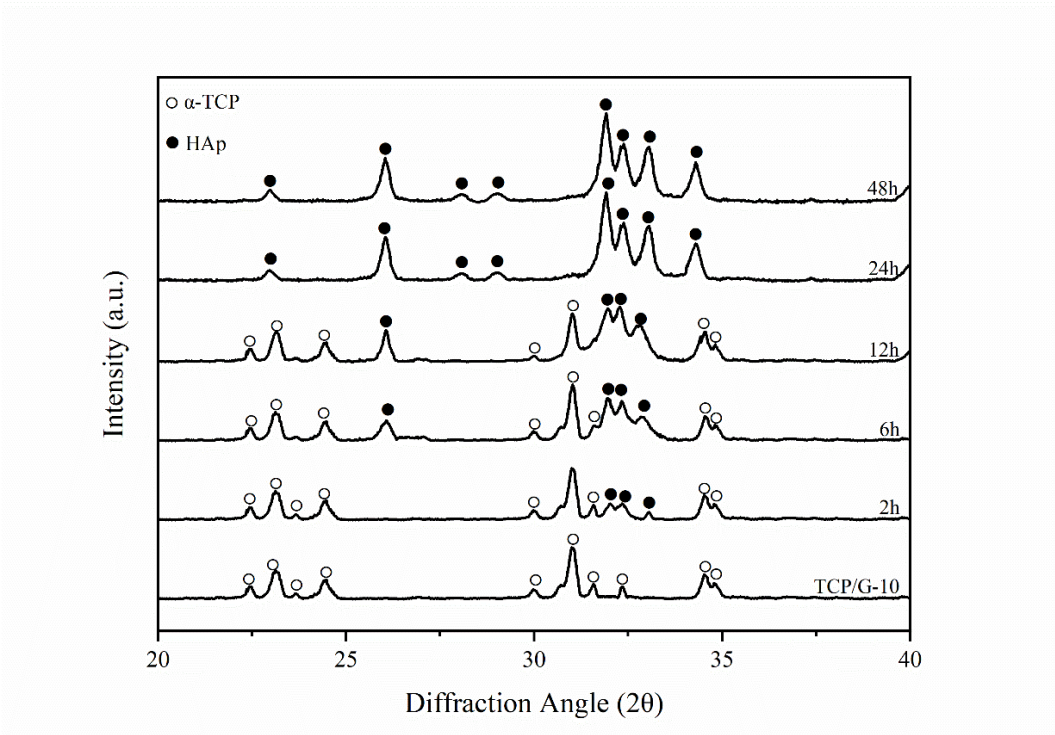



Figure A.3: The XRD diffractograms as a function of reaction time for TCP/G-10 in DI water.

## B. TCP/Gelatin Hydration in PBS

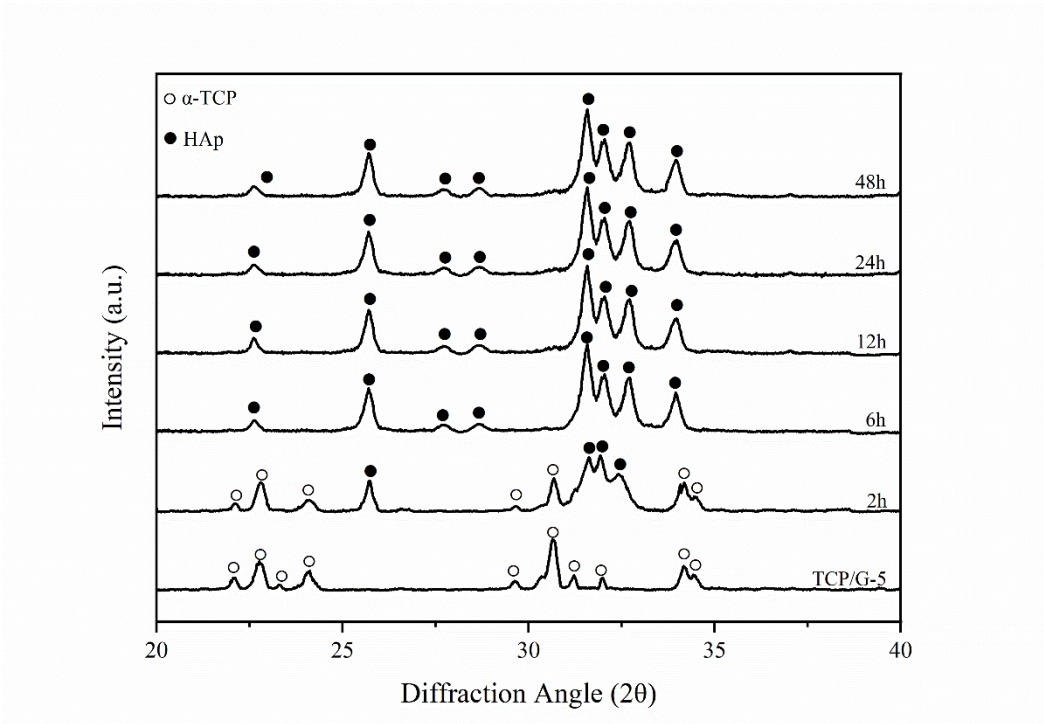



Figure B.1: The XRD diffractograms as a function of reaction time for TCP/G-5 in PBS.

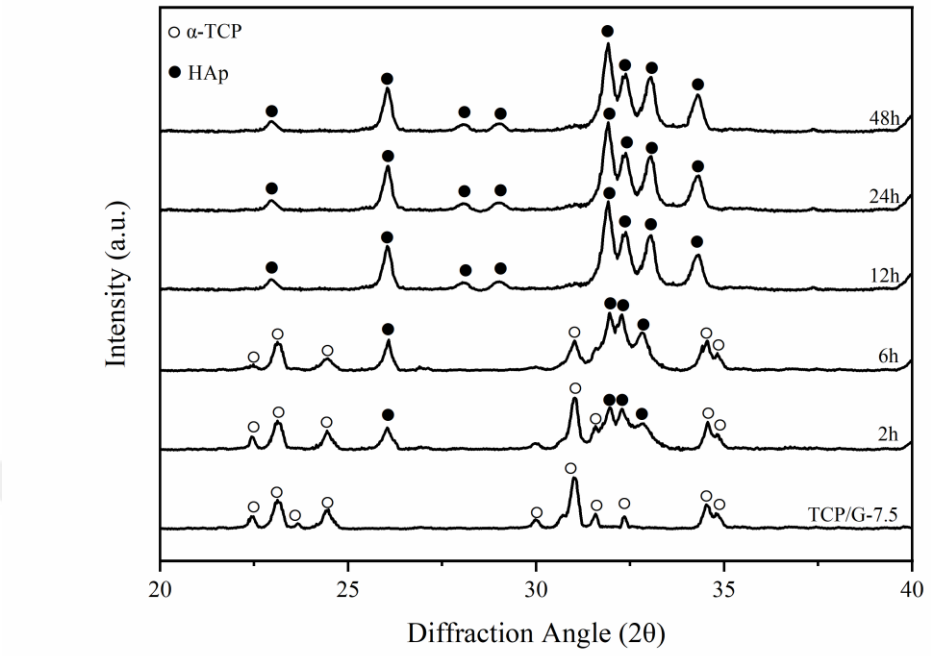



Figure B.2: The XRD diffractograms as a function of reaction time for TCP/G-7.5 in PBS.

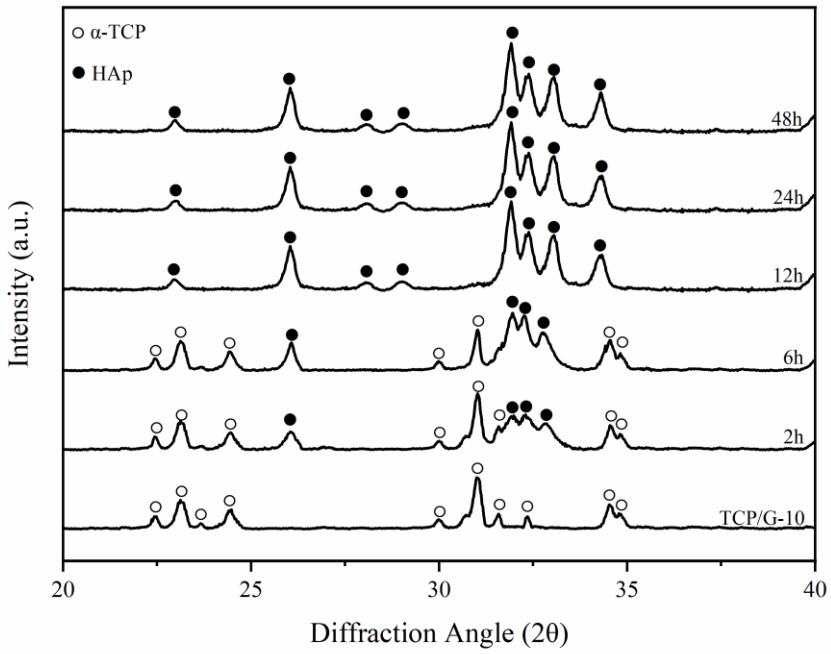



Figure B.3: The XRD diffractograms as a function of reaction time for TCP/G-10 in PBS.